frontiers | Frontiers in Materials

TYPE Review
PUBLISHED 15 October 2024
DOI 10.3389/fmats.2024.1453744

OPEN ACCESS

EDITED BY
Pavel Zelenovskii,
University of Aveiro, Portugal

REVIEWED BY
Takeo Sasaki,
Tokyo University of Science, Japan
Yuriy Garbovskiy,
Central Connecticut State University,
United States

*CORRESPONDENCE
Ingo Dierking,
ingo.dierking@manchester.ac.uk

RECEIVED 23 June 2024
ACCEPTED 11 September 2024
PUBLISHED 15 October 2024

CITATION
Aljohani O and Dierking I (2024) Modern developments in lasing with liquid crystals. *Front. Mater.* 11:1453744.
doi: 10.3389/fmats.2024.1453744

Modern developments in lasing with liquid crystals

Omar Aljohani[1,2] and Ingo Dierking[1]*

[1]Department of Physics and Astronomy, University of Manchester, Oxford, United Kingdom,
[2]Department of Physics, College of Science, Taibah University, Yanbu, Saudi Arabia

A review of the recent developments in the field of lasing with liquid crystals (LCs) is presented. After an introduction into the principle of lasing the different relevant liquid crystal phases to the field are introduced, namely, the nematic and chiral nematic phase, Blue Phases, twist grain boundary and ferroelectric liquid crystals. The classic examples of liquid crystal lasing are shortly discussed, together with a variety of possibilities for tuning the lasing wavelength, before the modern trends in LC lasing are discussed in detail. These are particularly random lasers, where the effects of nanoparticles, quantum dots and solitons are highlighted, as well as localized surface plasmon resonance. Other modern laser systems that have attracted recent interest, white lasers, whispering gallery mode lasers and those with biological materials, for example, cellulose nanocrystals, are also introduced and the latest developments outlined.

KEYWORDS

liquid crystal, laser, cholesteric, blue phase, composites, hybrid materials, biological materials

1 Introduction

The invention of the laser (Light Amplification by Stimulated Emission of Radiation) goes back about 7 decades, when Schawlow and Townes presented the theoretical groundwork (Schawlow and Townes, 1958) and Maiman published the first experimental demonstration of a working laser in 1960 (Maiman, 1960). The field of liquid crystals goes back considerably further into the 19th century, when Reinitzer discovered compounds that exhibited "two melting points" in 1888 (Reinitzer, 1888) and Lehmann coined the term "liquid crystal" already 1 year later (Lehmann, 1889; Coles and Morris, 2010). Thus, while the theoretical foundation and patent were established earlier (Goldberg and Schnur, 1973), the experimental work by Ilchishin and his colleagues in 1980 was the first successful realization of a liquid-crystal laser (Ilchishin et al., 1980). Since then, there have been about 1000 papers published on lasing with liquid crystals. The topic is now an established field of liquid crystal research, with a constant stream of work being published.

The field of lasing with liquid crystals has been rapidly developing in recent years. This is due to the fact, that the use of soft matter, of which self-organised, partially ordered phases such as liquid crystals are an essential part, offer the possibility of a changing photonic band gap (PBG) as lasing cavity and thus allow easy and dynamic tuning of the lasing wavelength. This is of elevated interest for scientists and engineers both fundamentally and for novel applications. With this review we aim to present an overview of the current state-of-the-art of the topic of lasing with liquid crystals.

In Section 1 we start with a short introduction to the principle of lasing and the structure and properties of liquid crystals, before introducing the established body of work on liquid crystal lasing in Section 2. This includes the cholesteric phase, the Blue Phase, the ferroelectric chiral smectic C* phase, cholesteric elastomers and a variety of

successful tuning mechanisms of the lasing wavelength. Section 3 discusses liquid crystal-based random lasers, the effect of nanoparticles, quantum dots in polymer dispersed liquid crystal composites, solitons–or so called nematicons, and localized surface plasmon resonance. Further modern developments are detailed in Section 4 on white light liquid crystal lasers and Section 5 on whispering gallery mode lasers based on liquid crystalline systems. Bio-derived liquid crystal materials for lasing are introduced in Section 6 with nematic filled butterfly wings as random lasers, lyotropic cellulose-nanocrystal based lasers and DNA in liquid crystal lasers.

The review is concluded by an outlook which discusses possible further developments in the field of liquid crystal-based lasing.

1.1 Laser principle

From an engineering perspective, lasers consist of three main parts: the cavity (resonator), the active media, and the pumping power (Nambiar, 2006). Liquid crystal (LC) materials contribute mainly to the cavity design and can also be used as part of the active media, such as dispersing a laser dye in the LC material (Khoo, 2022). There are several types of cavities, including the Fabry-Perot cavity, distributed feedback (DFB), distributed Bragg reflector (DBR), or scattering cavities (Khoo, 2022). The role of the cavity is to confine and amplify light by resonating it multiple times to generate coherent light. A typical cavity, such as the Fabry-Perot one, consists of two mirrors. In contrast, LC-based cavities are mirrorless, allowing easy tuning of the lasers (Khoo, 2022). Although DFB and DBR cavities are traditionally made of semiconductors, LC materials offer a replacement for the semiconductor's periodic structures either partially or fully in some lasers, enhancing the laser's efficiency and properties (Nambiar, 2006; Khoo, 2022).

The LC DFB cavity is made of LC phases that provide a periodic structure and are doped with active media (Nambiar, 2006; Mysliwiec et al., 2021). Similarly, two photonic LC phases, such as the cholesteric and blue phases, sandwich active media in DBR LC cavities (Nambiar, 2006; Mysliwiec et al., 2021). Another important cavity is LC random scattering cavities, which use scattering particles for optical feedback instead of traditional mirrors or distributed feedback structures (Nambiar, 2006; Mysliwiec et al., 2021). Another type, Whispering Gallery Mode (WGM) cavities, are typically ring-shaped and employ total internal reflection along the circular boundary to continuously trap light, providing a highly coherent laser output (Mysliwiec et al., 2021). These four main LC cavities (DFB, DBR, random scattering, and WGM) have broadened the applications of lasers.

Fundamentally, there are two, three, and four energy-level systems that describe the population inversion in lasing processes (Figure 1A) (Siegman, 1986). Practically, only the three and four-energy levels systems are able to achieve the population inversion and produce lasing (Milonni and Eberly, 2010). Population inversion, where more electrons are in the excited state than in the ground state, is necessary for lasing (Milonni and Eberly, 2010). When the laser cavity is optically pumped, particles absorb the incident optical energy, energizing electrons to a higher energy level. For lasing to occur, the number of electrons in the higher energy level must exceed those in the lower level. Incoming photons then stimulate these excited electrons, causing them to drop to a lower energy level and release additional photons with the same frequency, wavelength, phase, and direction as the incoming stimulating photons (Milonni and Eberly, 2010). By repeatedly exciting electrons and stimulating photons, the intensity of the light is amplified. Photons are amplified as they pass through optical cavities or mirrorless cavities like those found in liquid crystal photonic phases (Siegman, 1986). At the edge of the cavity, where the mirror is partially reflecting light, the amplified light escapes as coherent laser light if the stimulated emission exceeds the losses in the system (Siegman, 1986). The threshold condition is the point at which the gain medium's amplification of light cancels out all losses in the laser cavity (Svelto and Hanna, 2010; Liu et al., 2021). The primary forms of losses are internal (absorption and scattering), external (mirror and output coupling losses), diffraction losses, and non-radiative losses (Liu et al., 2021). To accomplish lasing, the gain in the laser medium must exceed all other losses in the system. The threshold condition is theoretically stated as a balance of gains and losses. The threshold gain coefficient g_{th} is given by:

$$g_{th} = \frac{1}{l}\left(\alpha_{total} + \ln\left(\frac{1}{R_1 R_2}\right)\right) \quad (1)$$

where l is the gain medium length, α is the total loss coefficient per unit length, including internal and external losses (Svelto and Hanna, 2010; Liu et al., 2021). $R1\,and\,R2$ are the two mirror reflectivities constructing the laser cavity (Liu et al., 2021).

Beside the stimulated emission, photon amplification can also occur through nonlinear optical (NLO) processes such as second harmonic generation (SHG) and optical parametric oscillators (OPOs) (Mysliwiec et al., 2021; Khoo, 2014). In linear systems, the induced polarization is proportional to the electric field. The dielectric constant and optical susceptibility are constants for every medium, regardless of the electric field. However, as the intensity of light traveling through the material increases, these constant relationships no longer hold, leading to the occurrence of nonlinear effects summarized in (Figure 1B) (Khoo, 2014; Zhou et al., 2020).

These levels (Figure 1B) are not energy eigenlevels of the unbound atom but rather represent the combined energy of one of the atom's energy eigenstates with one or more photons from the radiation field. Liquid crystals have special characteristics that can be used for nonlinear optics and dynamic tunability (Khoo, 2014). They can display nonlinear optical features, particularly when doped with suitable molecules for enhancing nonlinear responses or when subjected to electric fields (Khoo, 2014). Furthermore, LCs can be combined into optical cavities to provide dynamic tuning and modulation capabilities (Milonni and Eberly, 2010; Khoo, 2014). They are especially attractive for investigating nonlinear optics and designing photonic devices and applications due to their variable molecular ordering and significant optical nonlinearities (Khoo, 2014).

1.2 Liquid crystals

Liquid crystals (LCs) are fluids that exhibit flow properties and, at the same time, anisotropic physical properties, for example, the refractive

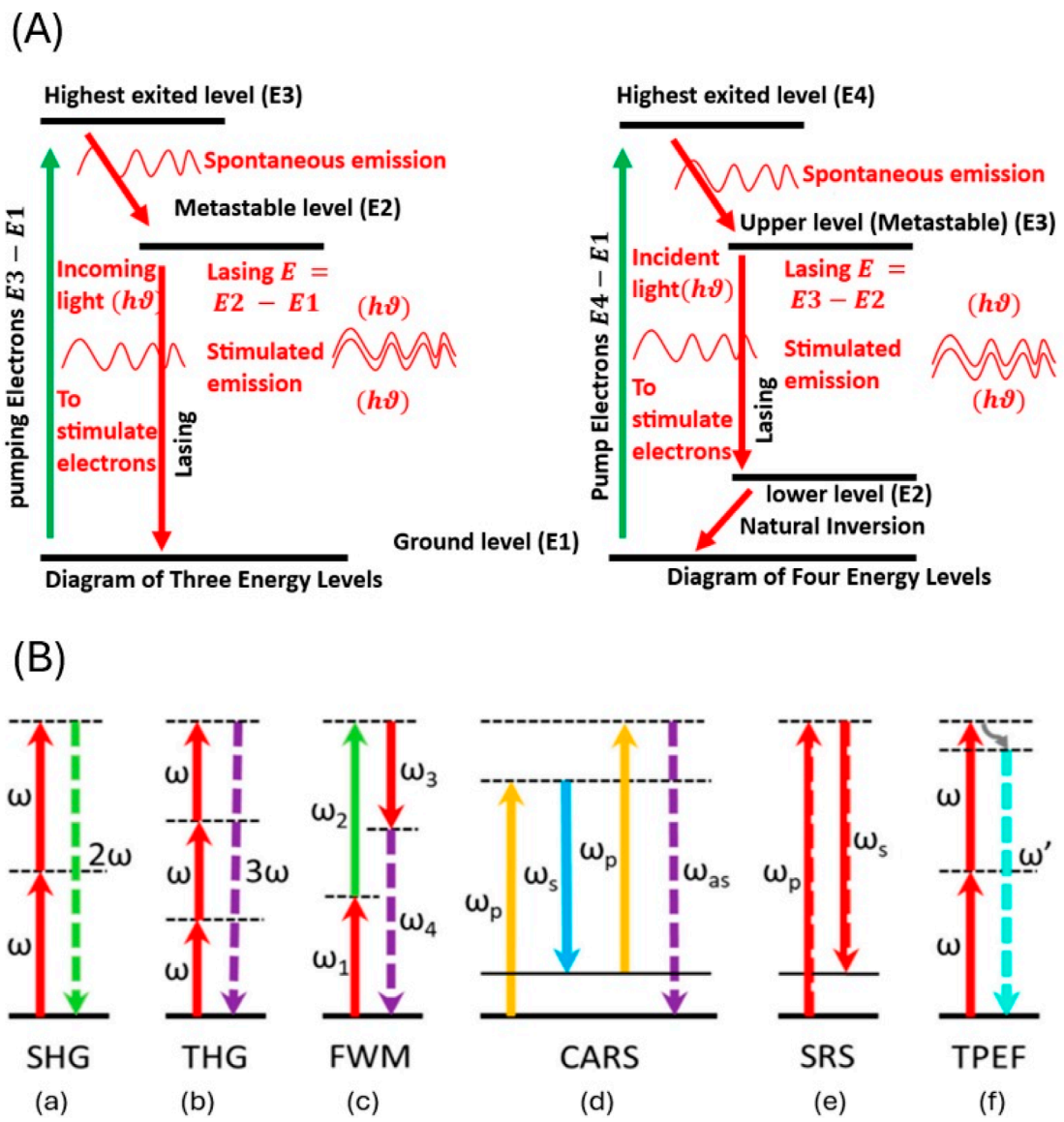

FIGURE 1
(A) Schematic illustration of the three and four energy levels of the system in lasing. **(B)** Schematic energy level diagrams for the nonlinear optical processes: **(A)** Second Harmonic Generation (SHG), **(B)** Third Harmonic Generation (THG), **(C)** Four-wave mixing (FWM). **(D)** Resonant Coherent Anti-Stokes Raman Spectroscopy (CARS). **(E)** Stimulated Raman scattering (SRS). **(F)** Two-Photon Excited Fluorescence (TPEF). The thick black solid lines depict the ground state, thin black solid lines represent the real electron or vibration energy state, and dashed lines represent virtual states. (Reproduced from (Zhou et al., 2020) under CC BY 4.0).

index, the dielectric constant, viscosity, *etc.*, Are direction dependent, as is commonly only observed for crystals (Schawlow and Townes, 1958; Maiman, 1960; Coles and Morris, 2010). Often termed the fourth state of matter, liquid crystals exhibit low dimension order and are thermodynamically located between the solid and the isotropic liquid state. Normally, one distinguishes between thermotropic and lyotropic phases, achieving the first type solely through temperature variation, and observing the second type by varying the concentration of surfactants, anisotropic nanoparticles, or other dopants in a suitable isotropic liquid. The latter phases are mostly only slightly dependent on temperature. In this paper, we will mainly concentrate on thermotropic liquid crystals, although lyotropic systems will occasionally also be mentioned.

Figure 2 depicts the most common phases observed. Starting with the isotropic phase at high temperatures, Figure 2A depicts the achiral, non-helical versions of these phases, while Figure 2B shows the chiral ones, which are of relevance to liquid crystal lasing. The isotropic phase exhibits neither orientational nor positional order and is thus equivalent to any other normal liquid. The only difference between this phase and the achiral phase, would be the observation of optical activity due to molecular chirality in the absence of any structural chirality. Only chiral materials exhibit a frustrated phase, known as the blue phases (Bagchi et al., 2023). These exist between the isotropic and the cholesteric phases and can occur in three different structural variants: BPIII, an amorphous

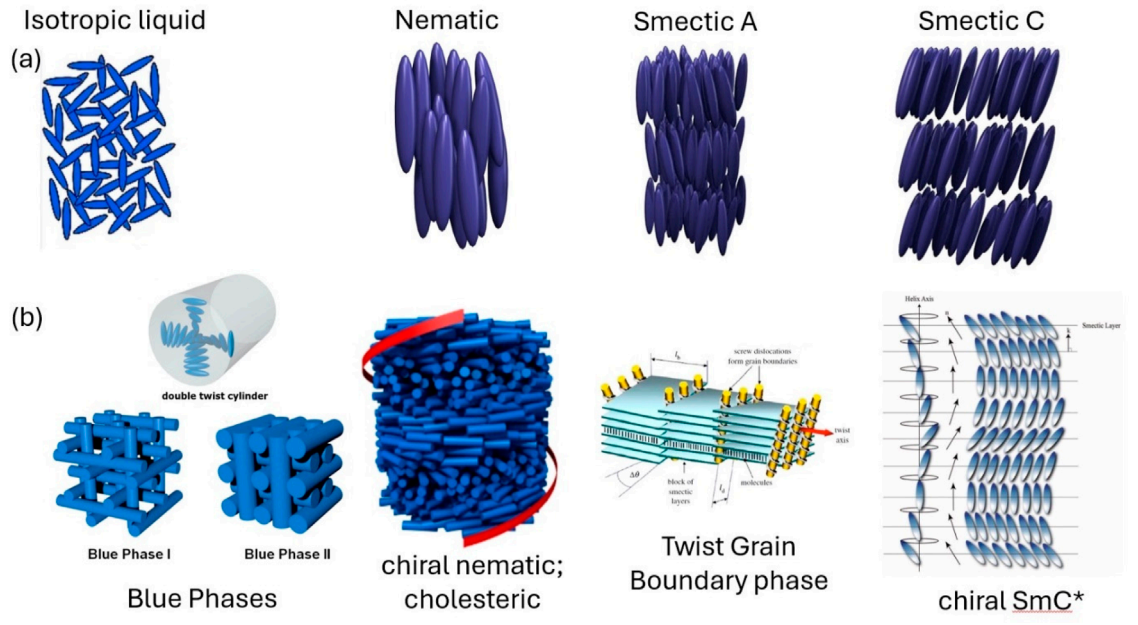

FIGURE 2
A schematic summary of the most common liquid crystal phases on cooling from left to right (Reproduced from (Dierking, 2014) under CC BY 3.0), . Part **(A)** shows the achiral version of the respective phases (Dierking, 2014), while part **(B)** shows their chiral equivalents, and in addition, the phases that can only be observed for chiral systems, i.e., blue phases, BP, and twist grain boundary phases, TGB. (Images of BP from (Sala-Tefelska et al., 2018) (With permission from Elsevier), cholesteric reprinted with permission from (Popova et al., 2016) (© American Chemical Society click here.), TGB Reproduced with permission from (Goodby, 2012) (© The Royal Society), and SmC* reproduced from (Ford et al., 2006) with permission. © 2006 Elsevier Ltd).

phase with local cubic order of defects; BPII, with a simple cubic unit cell of double twist cylinders; and BPI, with a body-centred cubic unit cell. The helical pitch of the double twist cylinders is generally of the order of visible light, often about 400–450 nm, hence the name of the phase. These phases are generally only stable over small temperature regimes of approximately 1K, but they have been used in 3D photonic systems with lasing action, which will be discussed below.

For achiral materials, the highest temperature phase that is observed is the nematic phase, with solely the orientational order of the long axis of elongated, rod-shaped molecules, while the centres of mass are isotropically distributed (Figure 2A). The chiral equivalent is the cholesteric phase, N*, which exhibits a one-dimensional helical superstructure (Figure 2B). The helical twist sense can be left- or right-handed, depending on the configuration of the chiral element of the LC molecules. The cholesteric phase's pitch is often of the order of visible light, but it can increase to several tens of micrometres. Additionally, researchers have demonstrated laser action with liquid crystals using the latter phase, as illustrated below.

Further cooling results in the formation of smectic phases, which, in addition to the orientational order of the long molecular axis, also exhibit a one-dimensional positional order of the centres of mass. As a result, these fluid smectic phases can be viewed as one-dimensional crystals or two-dimensional fluids. The high-temperature fluid smectic phase is called smectic A (SmA), where the long molecular axis (the director) is oriented along the smectic layer normal (Figure 2A). Composing this phase of chiral molecules results in molecular chirality, thus optical activity. However, if the system is highly chiral, particularly between the cholesteric and the smectic A* phase, we can observe a frustrated phase with a mostly narrow temperature range, exhibiting a helical superstructure. We refer to these phases as Twist Grain Boundary Phases (TGB) (Goodby, 2012), which, like BPs, are not present in every chiral liquid crystal. The helical superstructure's twist is discontinuous and can be commensurate as well as incommensurate. The pitch is generally of the order of a few hundred nm to tens of μm. Finally, a temperature-dependent tilt angle (Figure 2A) can cause a symmetry-breaking phase transition to the tilted smectic C phase, tilting the director with respect to the smectic layer normal. This transition is often second order. Interestingly, this phase, when composed of chiral molecules, exhibits the occurrence of a spontaneous polarization; the smectic C* (SmC*) phase is thus a ferroelectric liquid crystal (FLC) (Guo K. et al., 2019), and is indeed probably the only fluid ferroelectric material known to man. The system couples the spontaneous polarization with the tilt angle, and to compensate for the spontaneous polarization, P_S, at short distances, it forms a helical superstructure. Over a single pitch, P_S rotates through 2π, thereby compensating (Figure 2B). The pitch of the helix is generally observed between a few hundred nm and tens of μm. Also, this phase has been used for liquid crystal lasing (see below).

Helical structures in liquid crystals have an optical property known as selective reflection, which was theoretically derived by deVries (de Vries, 1951) for normal incidence when applying Maxwell's equations to helical birefringent media. Depending on the pitch P, a wavelength λ_0 is reflected for normal incidence onto the helix axis, given by $\lambda_0 = \langle n \rangle P$, where $\langle n \rangle$ is the average refractive index. The width of the reflection band is $\Delta\lambda = \Delta n P$, where Δn is

the birefringence. Later, selective reflection was also calculated for the incidence of other angles (Berreman and Scheffer, 1970) and arbitrary angles of incidence (Dreher et al., 2007).

Liquid crystals exhibit a variety of other hexatic, higher-order, and crystalline smectic phases, but these are not yet relevant to the topic of this paper.

Having provided a basic introduction to the principles of lasing and the structure and properties of the relevant liquid crystal phases, we can now proceed to a discussion how liquid crystal lasers perform for various LC phases and how laser tuning can be achieved.

2 Liquid crystal lasing

The liquid crystalline phases or materials where lasing has mainly been demonstrated are those composed of chiral molecules with a helical superstructure, where the pitch length, i.e., the length over which a 2π-twist of the director field is observed, can act as a resonator and provide the gain needed, together with doped dyes, to achieve the threshold for lasing (Kopp et al., 1998). The intriguing advantage of a liquid crystal laser lies in its ability to tune laser emission through various internal and external factors, thereby achieving miniaturization in the form of micro-lasers. Some of these structures and their lasing performance will be discussed in this part before we venture into the modern developments in liquid crystal lasing.

2.1 The cholesteric phase

Naturally, the first material to demonstrate lasing was the cholesteric phase, with its characteristic selective reflection and photonic band gap (PBG), often observable in the visible range of the spectrum (Ilchishin et al., 1980). After 2 decades from the first LC laser, Kopp et al. (Kopp et al., 1998) experimentally demonstrated the lasing phenomenon in 1998 using a dye-doped cholesteric structure at the photonic stop band. Kopp et al. showed the transmittance and reflectance in the visible part of the spectrum, along with the laser emission line at approximately 580 nm. Figure 5A depicts another example of a miniaturized lasing device (Varanytsia et al., 2019). The fluorescent dye-doped cholesteric liquid crystal is pumped by an SSY-1 Nd:YAG laser head at 532 nm after the original wavelength of 1064 nm passes a second harmonic generation (SHG) crystal. The pump wavelength is situated at the lower wavelength, higher energy end of the cholesteric reflection band, while the lasing line is observed at the higher wavelength, lower energy end of the reflection band at 607 nm (Varanytsia et al., 2019). The right part of Figure 3A shows the far field lasing emission pattern from the 23 μm-thick cholesteric cell (Varanytsia et al., 2019).

A range of dye-doped cholesteric systems were investigated in the past, all the way to the present day (Lin et al., 2024), also with combinations of different dyes (Shirvani-Mahdavi and Ebrahimi-Azandariani, 2019). Different wavelength regimes have been covered, ranging from the near IR to mainly the optical wavelengths, all the way into the region of UV light (Palffy-Muhoray and Taheri, 2001). Researchers have realized systems with low lasing thresholds for dye-doped cholesterics (Matsuhisa et al., 2007; Uchimura et al., 2010). Concepts have been developed to stabilise cholesteric lasing systems, for example, through the transition into a glassy state (Furumi and Tamaoki, 2010) or free-standing polymer films with a helical superstructure formed from cholesteric material (Matsui et al., 2002).

A different approach is polymer network formation (Schmidtke et al., 2002; Schmidtke et al., 2003), which effectively leads to a cholesteric gel known as polymer stabilised liquid crystal (PSLC). These are bi-continuous systems with a continuous polymer network in a liquid crystal phase. To achieve such systems, a bifunctional photo-polymerizable monomer is added in low concentration to a fluid in the dye-doped cholesteric phase. The monomer adopts the helical superstructure of the liquid crystal phase, which is then templated through photopolymerization. As a result, the lasing material stabilizes, with lasing properties that are very similar to those of the non-stabilised cholesteric LC.

On the contrary, at high monomer concentrations, polymer dispersed liquid crystal (PDLC) systems are formed during polymerization (Shibaev et al., 2003). A continuous polymer matrix is formed in which droplets of cholesteric LC are phase separated and dispersed. Such a PDLC's lasing behaviour is drastically different from that of the PSLC. While in the latter, a single laser line is observed at the edge of the photonic band gap (PBG), the former displays a range of different laser lines across the bandgap, which we will discuss in more detail in the following part of this paper.

2.2 The blue phase

As pointed out above, blue phases exhibit a cubic symmetry of defects, formed by a 3D lattice of double-twist cylinders. A typical platelet texture of the simple cubic BPII is observed with different colours corresponding to various lattice planes. To demonstrate lasing from the 3D photonic structure of the Blue Phase (Cao et al., 2002), a dye with a broad fluorescence peak at a centre wavelength of about 610 nm was dissolved in the liquid crystal, and the system was pumped with a Nd:YAG laser at 532 nm. The lasing intensity was measured in three orthogonal directions. Since the BP has a 3D photonic band gap (PBG), the authors measured the lasing intensity in three orthogonal directions (x, y, z). They observed strong laser lines developing at around 617 nm once the pump threshold of 75 nJ per pulse was exceeded, due to the reddish texture of the BP platelets. The highest lasing emission intensity was recorded at 98 nJ per pulse (Cao et al., 2002).

As expected, at low pump energies, the fluorescence spectrum is observed, with a laser line developing rapidly as the pump threshold is exceeded at approximately 75 nJ per pulse of duration 7.5ns (Cao et al., 2002). Lasing in all three directions is observed for a wavelength of approximately λ = 617nm, which is close to the wavelength of strong reflection at 611 nm.

In random lasing, the optical feedback mechanism is based on multiple scattering instead of conventional mirrors, which means that disorder is used to enhance the stimulated emission from a material (Sapienza, 2019). Also in blue phases and in polymer-stabilized blue phases (PSBPs) random lasing could be demonstrated (Chen et al., 2012). Polymer stabilisation of BPs has in fact raised much attention because of the possibility of substantially widening the temperature range of the otherwise very narrow BP. This has

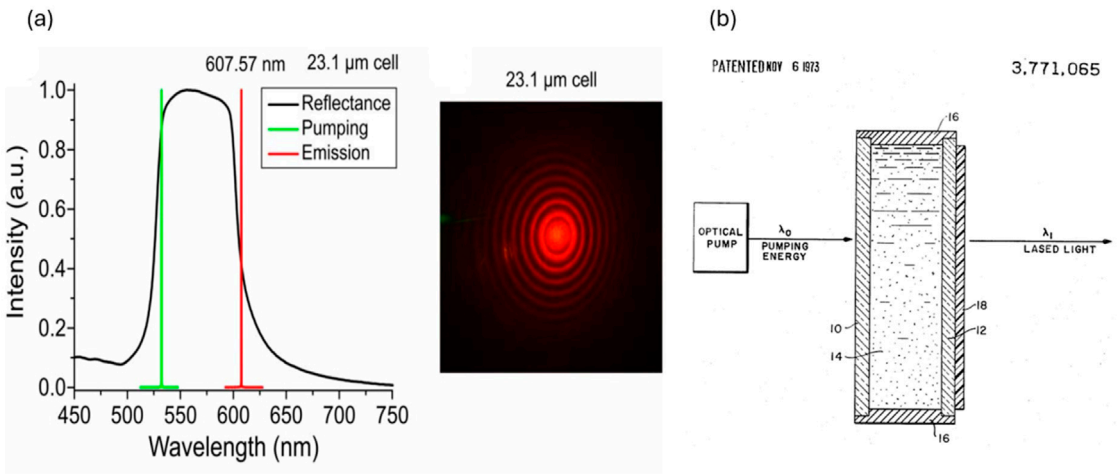

FIGURE 3
(A) Lasing of a pumped fluorescent dye-doped cholesteric liquid crystal and far field lasing emission pattern (Varanytsia et al., 2019). (Figure reprinted with permission from (Varanytsia et al., 2019). © Optical Society of America). **(B)** Sketch of the cholesteric liquid crystal laser device from the original US patent of 1973 (Goldberg and Schnur, 1973).

been exploited on several occasions, including in the development of PSBPs materials for lasing (Yokoyama et al., 2005; Wang et al., 2017) where temperature regimes of a width of approximately 30K were achieved around room temperature, in which the lasing emission wavelength as well as the lasing threshold energy were practically constant (Yokoyama et al., 2005). Furthermore, BP-templated 3D nanostructures have been fabricated, with the blue phase removed and refilled with a non-chiral nematic to still observe lasing activity (Castles et al., 2012). A mixture of a rod-like nematic and a bent-core smectic phase together with a chiral dopant has been reported to exhibit lasing from a large area, well aligned blue phase (Kim et al., 2015).

2.3 The ferroelectric chiral smectic C* phase

The possible occurrence of ferroelectricity in liquid crystals was predicted by the use of symmetry arguments. Meyer inferred that all tilted chiral smectic phases should possess a spontaneous polarisation P_S. If this polarisation is switchable between two stable states, we speak of ferroelectricity or ferroelectric liquid crystals (FLC). This was first demonstrated in 1975 for the smectic C* phase (Meyer et al., 1975). Compensation of P_S leads to the formation of a helical superstructure, which gives rise to a photonic band gap (PBG) similar to that of the cholesteric phase (Martinot-lagarde et al., 2011).

A first experimental demonstration of mirror-less lasing from a dye-doped FLC was published by Ozaki et al. (2002), which also showed that the laser line could be slightly adjusted by changing the temperature of the liquid crystal material, which in turn influenced the pitch. The range of tuning is rather small, approximately 20–30nm, because the SmC* pitch is generally practicably temperature-independent, except in a small range of temperatures close to the high temperature phase transition.

Kasano et al. conducted a study on mirrorless lasing using dye-doped FLCs in 2003 (Kasano et al., 2003). The emission spectrum of the laser clearly shows a laser line at approximately 480 nm (blueish green). For low pump energies below the threshold for lasing, an increase in emission intensity is observed due to spontaneous emission with a broad linewidth of approximately 80 nm. At the lasing threshold of about 10μJ/pulse the emission intensity strongly increases, while at the same time the emission linewidth reduces to about 0.5nm, that of a sharp laser line. It has been shown that the emission linewidth strongly decreases from 80 nm to 0.5 nm as the lasing threshold is exceeded, indicating laser action. Also here, it was reported that the laser wavelength could be slightly tuned this time by the application of an electric field by a total of 15 nm for fields of 0.25 Vm^{-1}. Very similar results were obtained in other publications (Matsuhisa et al., 2006a; Haase et al., 2007; Matsuhisa et al., 2006b). A comparison between cholesteric and FLC lasing (Ford et al., 2004) concluded that the overall lasing characteristics are in fact rather similar between the two phases and that there is not much difference between the two laser active materials, except that the lasing threshold for FLC materials is significantly lower than for the cholesteric materials, which was attributed to the increased order of the smectic phase.

2.4 Cholesteric elastomer films

Above, we have mentioned a few cholesterics and blue phases polymer systems as they are used for liquid crystal lasers, namely, polymer stabilised systems (PSLCs) and polymer dispersed systems (PDLCs). The former are phase-separated bi-continuous materials where a polymer network percolates through the liquid crystalline phase similar to a gel, while the latter are phase separated systems with liquid crystal droplets being dispersed in a continuous polymer matrix. Both do not significantly respond to stress, with strains being small for PDLCs and fractures being observed for even small stresses in PSCTs.

Based on the original idea of Palffy-Muhoray, Finkelmann et al. (Finkelmann et al., 2001) synthesised cholesteric elastomers and

lasing was demonstrated with a slightly different concept: cholesteric elastomers, basically cross-linked rubber-like materials with the anisotropic order of the liquid crystal phase (Finkelmann et al., 2001). These elastomers respond strongly to applied stresses and provide a strain of about 100% or even more. A spectrum of a cholesteric dye-doped elastomer was observed after being pumped by a frequency-doubled Nd:YAK laser at λ = 532 nm with 35 ps pulses (Finkelmann et al., 2001). The sample, a free-standing elastomer, is undeformed and shows a broad fluorescence emission below the pump energy threshold of 280 μJ (Finkelmann et al., 2001). Line narrowing was observed on approaching the lasing threshold, and at higher energies, a sharp laser line is obtained at approximately 592 nm (Finkelmann et al., 2001). The elastomer in its deformed state was seen under white light illumination of a 0.25 mm thick film (unstretched) (Finkelmann et al., 2001). From stretched to unstretched, the strain decreases, and one can see that the cholesteric bandgap changes from blue *via* green to red, which is reflected by red shift the lasers emission (Finkelmann et al., 2001).

In another publication on a biaxially stretched elastomer film, it is found that the lasing threshold pump energy is of the order of 0.5 μJ and for larger values of the pump energy, the emission energy increases linearly until saturation (Schmidtke et al., 2005). As film deformation increases, the emission wavelength decreases to shorter values (Schmidtke et al., 2005). Corresponding results were in fact obtained recently for a Blue Phase elastomer (Zhang Y. S. et al., 2020).

2.5 Tuning of lasing wavelength

Being able to tune the wavelength of laser emission is one of the major advantages of liquid crystal lasing over other techniques involving organic gain materials or solid-state lasers. We will outline the most common techniques, and one can distinguish between passive and active control of the laser emission. As passive methods, one could consider those that allow a tuning of the emission wavelength during the fabrication of the liquid crystal mixture employed. Once this is done and the lasing cell is filled, the emission wavelength is determined and maintained. For example, the stop band can be influenced by the chiral dopant (or its twisting power) chosen to generate the cholesteric phase's pitch. Similarly, a chiral dopant concentration can be chosen to generate a specific pitch at a given temperature. These choices also influence the temperature dependence of the pitch, so that one can change the sample temperature to tune the wavelength of the emission line. An example of laser emission wavelength tuning for different concentrations of a chiral dopant (CB15) is depicted in Figure 4 (Palffy-Muhoray and Taheri, 2001). Huang, Y., et al. have tuned the laser emission line of a cholesteric by changing the temperature (Huang et al., 2006). A variation in temperature changes the position of the photonic stop band and hence tunes the wavelength of laser emission. In general, a decrease in wavelength is observed with increasing temperature (Huang et al., 2006).

Wide range tuning capability in the visible range of the spectrum was demonstrated by Lin et al. (Lin et al., 2005). This was even further enhanced covering the UV-VIS region by Chanishvili et al. (Chanishvili et al., 2005). It should also be mentioned that this

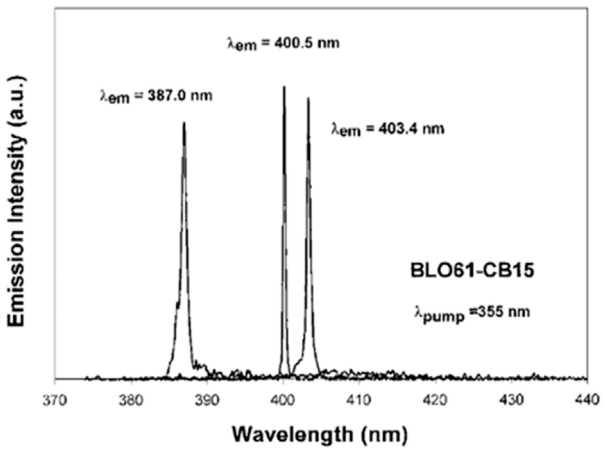

FIGURE 4
Tuning the laser emission line by varying the concentration of the chiral dopant in a cholesteric liquid crystal. A decreasing wavelength is observed for increasing dopant concentration (Palffy-Muhoray and Taheri, 2001). (Figure reproduced by permission from © Optica Publishing Group).

tuning strategy can also be employed for Blue Phases and polymer-stabilized BPs with good success (Hur et al., 2013; Mazzulla et al., 2012). For example, BP laser has been successfully tuned thermally for about 55 and 60 nm for two sample using two different dyes for BP stable for 150 nm (Hur et al., 2013).

An active method of tuning the lasing wavelength is to apply an electric field to the sandwich sample via transparent indium tin oxide (ITO) electrodes. Generally, the observed range of lasing wavelength variation is relatively small. For instance, lasing is tuned by about 15 nm for an electric field variation of 10 MVm^{-1} (Chanishvili et al., 2004).

At this point, it should be mentioned that a very similar tuning mechanism via electric field application can also be used for blue phases (Manda et al., 2020), although it appears that the tuning range is quite a bit more substantial, achieving a tunability Δλ of approximately 241 nm for electric field amplitudes of up to 7.1 Vum^{-1} (as it can be seen in Figure 5). Other examples for BP and (PSBPs) systems were reported by Chen et al. (Chen et al., 2015) and Liao et al. (Liao et al., 2019).

A more unconventional but very effective method for tuning the laser wavelength of a cholesteric is the introduction of a pitch gradient in the plane of the sandwich cell and subsequent translation of the pump beam to a position that generates the desired position of the photonic band gap (PBG) (Chanishvili et al., 2004). The pitch gradient is obtained by filling a cell from opposite sides with two different mixtures containing a different amount of chiral dopant. The pitch of the cholesteric structure can range from the UV spectrum at the top to the NIR spectrum at the bottom. This has been experimentally achieved by filling a liquid crystal cell with different concentrations of chiral dopant from opposite sides, creating a pitch gradient within the cell (Chanishvili et al., 2004). The applicability of this method has been demonstrated experimentally (Chanishvili et al., 2005) and can of course be utilised for other cholesteric and BP systems as well, as, for example, the glass forming

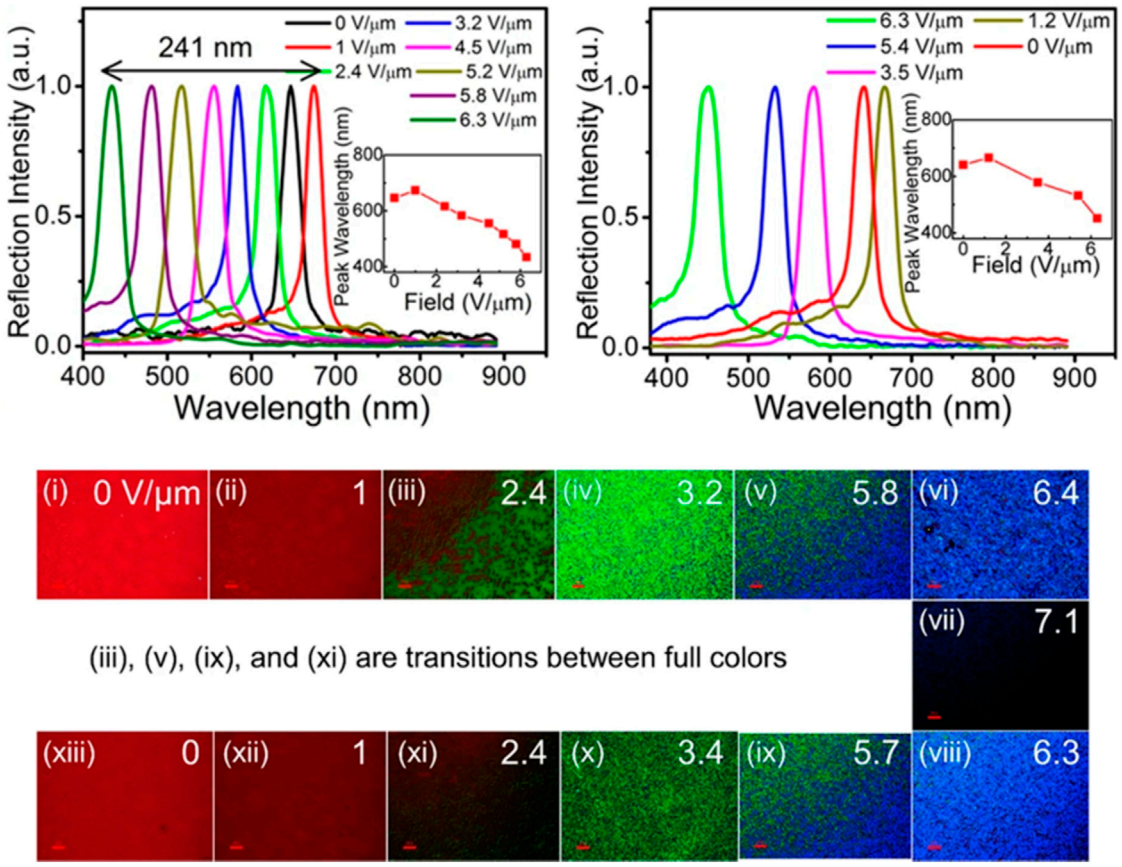

FIGURE 5
The left line graph shows the tuning of the photonic band gap (PBG) of polymer-stabilized blue-phase (PSBP) liquid crystals by increasing the voltage, while the right line graph illustrates the tuning of the PBG by decreasing the voltage. Below these graphs, the corresponding textures of the PSBP at each voltage are displayed (Manda et al., 2020).

cholesteric mentioned before (Furumi and Tamaoki, 2010) or Blue Phases (Liao et al., 2019; Lin et al., 2016).

Another tuning strategy was proposed in (Lin et al., 2006), which is based on the addition of a dye that undergoes a conformational change when illuminated with UV light. This conformational change causes a pitch variation with time of UV illumination and a red shift of the wavelength of selective reflection (Chanishvili et al., 2004). By translating the cell and thus directing the pump beam at different bandgaps, this method allows tuning of the laser wavelength through the whole visible spectrum (Chanishvili et al., 2005). This in turn leads to a tuning of the lasing wavelength between approximately 380–420 nm (Chanishvili et al., 2005). Very closely related to the use of UV sensitive dyes is the addition of a small amount of a material with an azo-group, which is often employed in liquid crystal photo-effects due to its trans-cis isomerization under illumination with UV light. The effect of illumination times, ranging from 0 to 15 min, on the cholesteric bandgap and lasing emission wavelength has been successfully achieved (Lin et al., 2005). The method can, of course, also be applied to different cholesteric and BP systems, for example, the glass forming material encountered before (Furumi and Tamaoki, 2010). A comprehensive study of the effect of azobenzene as a photo-dopant was published by Hrozhyk et al. (Hrozhyk et al., 2007).

As an example of using active electric field application in the tuning of laser lines of ferroelectric liquid crystals, we refer to paper (Matsuhisa et al., 2006a). The band gap due to selective reflection can clearly be seen as a dip in the transmittance curve, while the dye doped SmC* sharp laser line is located at the long wavelength end of the band gap at approximately 615 nm (Matsuhisa et al., 2006a). A clear threshold behaviour at a pump energy of 600 μJcm^{-2} is observed where lasing activity commences, as indicated by the sharp drop of the emission intensity half-width by more than two orders of magnitude (Matsuhisa et al., 2006a). Wavelength tuning from 595nm to 615 nm could be achieved by the application of a very moderate electric field of amplitude 0.14MVm^{-1} (Matsuhisa et al., 2006a). In this paper, the authors present the transmittance indicating the position of the SmC* optical band gap of the ferroelectric liquid crystal and emission intensity demonstrating laser action with a sharp line at approximately 615 nm. Moreover, the typical threshold behaviour for the pump energy and the line is observed for laser action. It has been demonstrated experimentally that the laser wavelength can be tuned over a range of approximately 20 nm with the application of relatively small electric fields (Matsuhisa et al., 2006a). Similar results have been reported in (Ozaki et al., 2004). Recently, a latest study successfully prepared a chiral ferroelectric nematic liquid

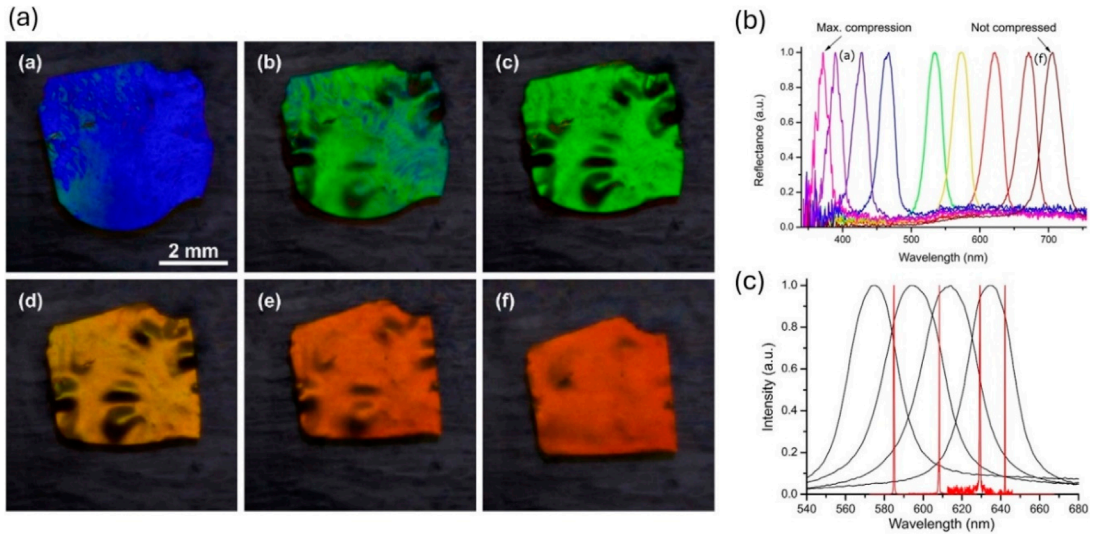

FIGURE 6
(A) Selective reflection observed from a cholesteric elastomer film illuminated by white light for decreasing strain from blue to red. **(B)** Corresponding measurements of the selective reflection spectra at maximum compression to the relaxed state. **(C)** Some of the laser lines are red-shifted during the relaxation process (Varanytsia et al., 2015).

crystal laser by combining the ferronematic compound RM734 with chiral dopants and the fluorescent dye PM597 (Folcia et al., 2024). The authors demonstrated the ability to reversibly tune the laser's wavelength by 30 nm through the application of an electric field (Folcia et al., 2024).

At last, we show the tunability of laser emission for a cholesteric elastomer by mechanically changing strain, as demonstrated by Varanytsia et al. (Varanytsia et al., 2015). A uniform uniaxial strain is applied along the helical axis, mechanically altering the helical superstructure's pitch. The compressed structure exhibits a selective reflection of incident white light at a short wavelength in the blue region of the spectrum. Relaxation of the uncompressed helix changes the wavelength of selective reflection through the visible spectrum to red (Figure 6A). This change is quantified in Figure 6B with spectra recorded during the relaxation process at different times, from maximum compression at t = 0 to uncompressed at t = 48 min. During this process, the wavelength of laser emission changes, being shifted to the red (Figure 6C, for clarity, not all lines corresponding to the selective reflection measurements are shown). It is found that both the wavelength of selective reflection as well as the laser emission wavelength change linearly with applied strain.

After this overview of the standard approaches to liquid crystal lasing and laser wavelength tuning, we will now discuss the recent modern developments in the field, starting with liquid crystal random lasers.

3 Random lasers

Random lasers (RLs) are lasers that do not use a standard optical cavity with mirrors to provide feedback. Instead, they use repeated scattering of light inside a disordered material to achieve the optical feedback required for lasing (Figure 7A). The unusual structure of RLs results in lasers with low spatial coherence, making them suitable for sensing applications (Qu G. et al., 2023; Padiyakkuth et al., 2022). Random lasers are classified into several types, including localized random lasers, diffuse random lasers, hybrid random lasers, random fibre lasers, colloidal quantum dot random lasers, nanoparticle-doped random lasers, liquid crystal random lasers (LCRLs), organic and polymer-based random lasers, and perovskite-based random lasers (Qu G. et al., 2023; Padiyakkuth et al., 2022; Azmi et al., 2022; Turitsyn et al., 2014).

Here, the current advances in LCRL research will be highlighted. Liquid Crystal Random Lasers use liquid crystals as a scattering medium. The liquid crystals' unique optical characteristics, including anisotropy and sensitivity to external stimuli, allow for precise control of the lasing characteristics. LCRLs may be precisely tuned by modifying their orientation and phase in response to external stimuli like electric fields, magnetic fields, or temperature changes (Qu G. et al., 2023).

3.1 Liquid crystal random lasers

A detailed study demonstrated that a number of parameters, including pump rates, the radius of nematic liquid crystal (LC) droplets, the filling fraction of nematic LCs, and the angle between the polarisation direction of the pump beam and the NLC director, all influence the properties of random lasers (Meng et al., 2022). It was shown that increasing the pump rate beyond the threshold of 4.7×10^7 s^{-1}, measured in terms of the number of photons or energy per second, led to an increase in both the intensity and the number of laser modes (Meng et al., 2022). The increase of pump power increases the spectral intensity as well as the random laser modes (Meng et al., 2022). Furthermore, the ideal radius for NLC droplets that maximizes the emission intensity is

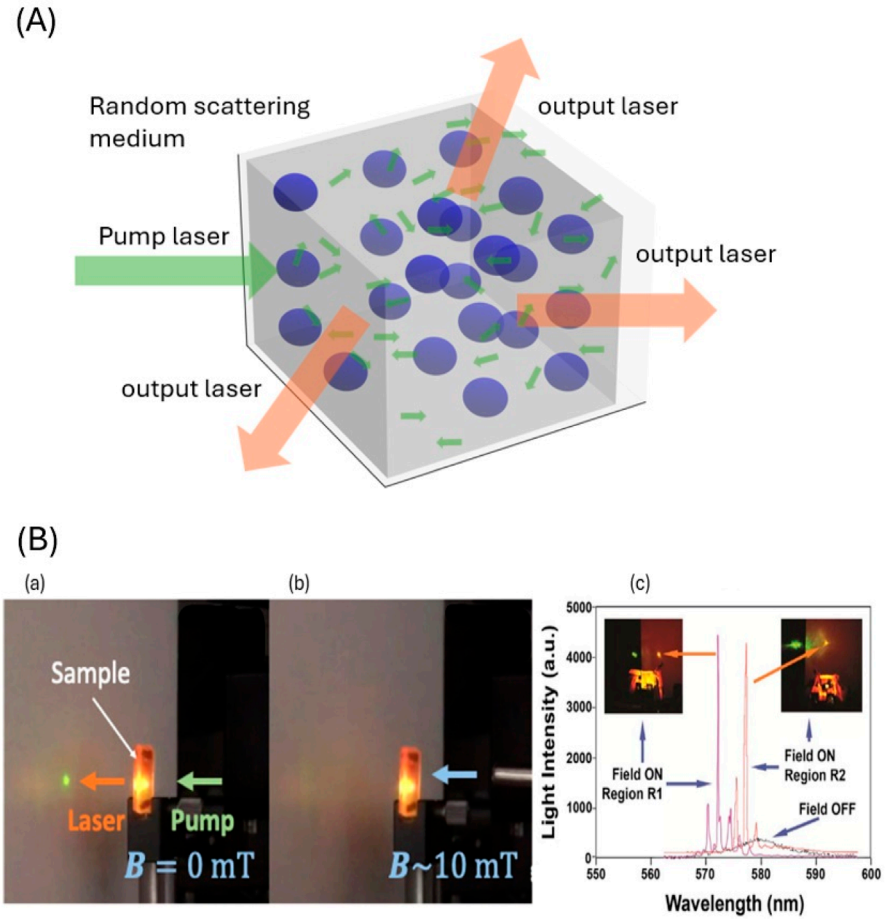

FIGURE 7
(A) Schematic illustration of the random laser scattering mechanism. **(B)** Switching of the random laser emission by applying magnetic and electric fields: **(A)** The random laser emission is visible on the screen with no magnetic field, while **(B)** the emission is extinguished when the magnetic field is applied perpendicular to the cell plane (Naruta et al., 2019). (Figures (a and b) reprinted with permission from (Naruta et al., 2019). © Optica Publishing Group). **(C)** Emission spectra of RL at an excitation wavelength of around 532 nm, with an 8 ns pulse width and around 500 μJ pulse, in the off state (black line) and in the on state at 16 V (R1, dot pink line; R2, solid red line) (Shasti et al., 2016). (Figure (c) Reproduced with permission from (Shasti et al., 2016). © The Optical Society).

approximately 75 nm (Meng et al., 2022). It was also demonstrated that the maximum emission intensity and number of laser modes occur when the polarisation direction of the pump beam is parallel to the nematic LC director (Meng et al., 2022). At a fixed nematic droplet radius of 50 nm, the spectral intensity increases as the pump rate passes the threshold and depends on the angle θ between pump beam polarisation and liquid crystal director (Meng et al., 2022). Another study illustrated that this effect is mostly due to the pump pulse-induced reorientation of the NLC direction. This reorientation improves light scattering, resulting in the observed nonlinear behaviour (Yao et al., 2016). The effect of applying different alignment or anchoring conditions as well as electric fields on RL emission, scattering, and polarization has been investigated. For instance, antiparallel rubbing, along with the application of an external electric field, influences the polarization of the random laser from dye-doped nematic liquid crystals (Ye et al., 2017a). The rubbing process made the laser linearly polarized, while increasing the applied electric field reduced the degree of laser polarization (Ye et al., 2017a). This tuning of the polarization benefits many applications related to polarization adjustment (Ye et al., 2017a). In addition, another study has constructed a random laser based on twisted nematic LCs (TN-LC) that serve as a random scattering cavity (Chen et al., 2017). The TN-LC is made in the standard procedure by rubbing the top glass perpendicular to the bottom glass, as shown in Figure 17 (Chen et al., 2017). The study examined the laser's mode stability and electrical switchability, as well as the correlations between the lasing threshold, alignment direction, dye concentration, and layer thickness (Chen et al., 2017). It was discovered that the polarization direction of dye-emitted light rotates along the 90^{O} twisted optic axis of the liquid crystal, resulting in output polarisation states parallel to surface alignment directions. In this study, the optimal dye concentration for low-threshold random lasing was determined to be 0.26 wt%, with a threshold of 1.13 μJ cm^{-2}.

Similarly, wedge cells were fabricated and filled with dye-doped twisted nematic liquid crystals (DD-TNLCs) to create polarized random lasers (RLs) (Lin S. H. et al., 2017). It was discovered that the wedge cell improved dispersion, which is required for good

random lasing results. The authors also achieved linear polarized random lasing beams emitted perpendicularly from both sides of a dye-doped twisted nematic liquid crystal wedge cell (Lin S. H. et al., 2017). Regarding the effect of electric field on polarization, a study has demonstrated the electrical controllability of the polarization direction of random lasing emitted vertically from a dye-doped nematic liquid crystal (NLC) (Yao et al., 2023). A slit of width 230 μm was created on the indium tin oxide (ITO) glass cell by etching the electrode, which enabled the formation of an electric field when a voltage was applied across the slit (Yao et al., 2023). At an applied voltage of 200 V (or 8.7×10^5 V/m), the polarization direction could be continuously tuned to reach a maximum rotation angle of approximately ninety degrees (Yao et al., 2023).

Further research developed a dye-doped nematic liquid crystal random laser (RL) and demonstrated a considerable increase in emission intensity above the Fredericks threshold due to enhanced light scattering on liquid crystal domains (Sznitko et al., 2016). Moreover applying a DC voltage and utilising a metalized diffraction grating, an increase in emission intensity and a red-shifted emission spectrum were observed (Sznitko et al., 2016).

Photonic band edge and random lasers based on chiral nematic liquid crystals with thermal switching capabilities were successfully developed (Lu et al., 2021). The photonic band-edge laser emission was accomplished by increasing the concentration of the chiral agent until the reflection band overlapped with the fluorescence spectrum. Increasing the pumping energy until it exceeded the lasing threshold of the photonic band gap (PBG) laser resulted in the observation of random laser emissions (Ye et al., 2018).

A cholesteric liquid crystal (CLC) random laser (RL) was fabricated by first aligning the liquid crystal molecules using an alternating current (AC) electric field, followed by stabilizing the structure through a polymer network formed *via* photopolymerization. The fabrication process began with the application of an AC electric field (150V, 1 kHz for 1 min) to the CLC, which aligned the helical structure of the liquid crystal. This alignment was then stabilized by creating a polymer network through UV irradiation (365 nm, 3 mW/cm^2) of bifunctional monomers within the liquid crystal, ensuring the structural integrity of the aligned molecules (Lu et al., 2021). The photonic band gap (PBG) contributes through selective reflection, while the polymer network enhances scattering (Lu et al., 2021). This combination results in a gradient distribution, widening the bandgap, and tuning the random laser wavelength.

For a comparative study, a dye-doped polymer-dispersed liquid crystal (DDPDLC) was constructed in two different cells, varying the boundary conditions in such a way that for one, the substrates were rubbed to achieve planar alignment layer on one side of the cell, leaving the other side unrubbed and the other cell without any alignment layer for either substrate (Ye et al., 2017b). This setup was used to study the effect of rubbing on random lasing emission. It was found that the cell with the rubbed planar alignment layer on one side had a lower threshold compared to the unaligned cell across different cell thicknesses.

In a recent study a planar defect was introduced on the surface of the cell by only rubbing one substrate to inhibit band-edge lasing through the photonic band gap (PBG) of the CLC (Lu H. B. et al., 2018). By leaving the texture of the LC prone to defects at one boundary only, the authors leveraged the unaffected internal PBG to enhance scattering and facilitate the creation of a random laser (Lu H. B. et al., 2018). They achieved thermal tuning of the RL wavelength over a wide spectral range (500–700 nm) by gradually applying near-infrared (NIR) irradiation at 850 nm as a controllable heat source (Lu H. B. et al., 2018).

Regarding the effect of monomer additives, after creating the DDPLC RLs, it was observed that a 20 wt% increase in monomer concentration produced stronger emission peaks and a lower lasing threshold (Lin and Hsiao, 2014). Moreover, higher pump energies typically lead to narrower linewidths and higher emission peaks, whereas higher temperatures have the reverse effect.

Further, another additive, which is a redox dopant for stabilising the LCRL enhancement, was investigated. A dye-doped LCRL laser was designed by using a combination of smectic A and nematic phases together with redox dopants that have an effect on the electrical properties (Khan et al., 2015). The introduction of redox dopants was shown to stabilise the dye in scattering mixtures, enhancing the long-term repeatability and stability of smectic A random laser emission.

The influence of phase transitions on random laser operation is an interesting topic. The behaviour of random lasing in different liquid crystal (LC) phases at increasing temperatures was examined in ref. (Trull et al., 2017). Initially, the RL operated in the Smectic B phase, a hexatic smectic phase, below temperatures of 320 K with a threshold of 1 MW/cm^2. Upon reaching temperatures between 320 K and 333.2 K, the phase transitioned to the fluid smectic A phase, with an RL threshold of 1.2 MW/cm^2. An additional temperature increases into the range of 333.2 K–348.9 K caused random lasing to occur in the nematic phase, with a threshold of 2.3 MW/cm^2. At temperatures higher than 348.9 K, in the isotropic phase, the random lasing threshold was obtained at 90 MW/cm^2. These findings demonstrate that the particular LC phase significantly influences the threshold and emission performance of random lasers (Trull et al., 2017).

Magnetic switching of random lasing was studied on a system of a random laser using dye-doped ferromagnetic nematic liquid crystals (FNLCs), which function as a randomly scattering cavity (Naruta et al., 2019). Magnetic nanoparticles (MNPs) (Sc-substituted barium hexaferrite (BaFe12-xScxO19)) were added to the NLC to adjust the random laser emission intensity by applying an external magnetic field. As the MNPs align with the nematic director due to surface anchoring interactions, applying an external magnetic field reorients both the MNPs and the NLC, coupling their directors. Consequently, the scattering changes, thus altering the random lasing feedback conditions (Naruta et al., 2019). Figure 7B, parts (a) and (b) clearly illustrate this.

A small magnetic field of about 1 mT can thus regulate the random laser's intensity. This is achieved by changing the direction and polarization-dependent emission of light in FNLCs in the presence of an external magnetic field (Naruta et al., 2019).

Moreover, as can be seen in Figures 7B, C, an electric field induces a random laser based on a dye-doped liquid crystal system with negative dielectric anisotropy, which was studied in ref. (Shasti et al., 2016). It was found that random lasing occurs when the electric field is applied, resulting in a planar-like structure with local nonuniformity in the liquid crystal orientation.

In a case of random lasing based on rare LC phases, a laser was fabricated based on a so-called sphere phase LC (SPLC),

which exists between the isotropic and the blue phases. This sphere phase is composed of 3D twisted spherical structures with line defects between them (Zhu et al., 2015). The increased scattering and interference from the 3D twisted spheres resulted in a 32% lower lasing threshold as compared to the chiral nematic phase.

Generally, scattering causes the output of the random lasing emission to become dispersed and less efficient. Therefore, recent research has explored various methods for waveguiding the emission. One attempt to solve this problem was to use electric fields to waveguide the RL emission. Nematic liquid crystal random lasers (NLCRLs) were enhanced by electrically guiding the emission waves (Huang et al., 2021). The waveguide effect improved control over RL properties and decreased transmission loss. Liquid crystal molecules (LCMs) were rotated by the electric field, which changed the polarisation and intensity of the RLs (Huang et al., 2021).

Using a fibre instead of the traditional glass slide LC cells broadens the application of LC RL by enhancing the lasing characteristics. For instance, a random laser was created using a photonic crystal fibre (PCF) that was filled with a dye-doped nematic liquid crystal (NLC) (Nagai et al., 2017). When the excitation polarisation was parallel to the PCF axis, the laser threshold was measured at 80 μJ/mm^2 per pulse (Nagai et al., 2017). This threshold is much lower than random lasers with dye-doped organic solvents in PCF that have been described in another study (Nagai et al., 2017). The high refractive index of the NLC, which increases the scattering efficiency, is responsible for the low threshold (Nagai et al., 2017). Similarly, researchers developed optically end-pumped liquid crystal random fibre lasers (LC-RFLs) (Yang et al., 2019). This configuration generates a gain channel with lossy cladding, resulting in coherent random lasing along the fibre axis. This unique laser source has low spatial coherence and excellent directionality, making it perfect for speckle-free imaging applications.

Moreover, a dye-doped liquid crystal random laser was controlled electrically at the glass cell and magnetically at the fibre (Ye et al., 2014). For electrical control, the threshold voltage for a cell gap of 188 μm was 4.54 V for no rubbing (NR), 3.7 V for one-side rubbing (OSR), and 2.8 V for two-side rubbing in the same direction (TSRS). For magnetic control, the introduction of a magnetic field raised the random laser's threshold, making lasing even harder under magnetic control (Ye et al., 2014).

3.2 Liquid crystal random lasers with nanoparticles

Studying the addition of nanoparticles (NPs) to dye-doped liquid crystal (DDLC) for random lasing enhancement is an important research area as the NPs provide a significant benefit to the LC laser action, such as stability, an increase in scattering, or variation options as a gain medium. In one of the studies, ferroelectric nanoparticles of barium titanate ($BaTiO_3$, 100 nm, n = 2.2) were dispersed into DDLCs to enhance random laser (RL) scattering (Lee et al., 2015). As shown in Figure 8, at a concentration of 0.3 wt% $BaTiO_3$, the lasing exhibited the highest RL performance compared to other concentrations (Lee et al., 2015).

Another study demonstrated switchable random lasers using a DCM dye laser as a gain medium, nematic liquid crystal elastomer (NLCE), and titanium dioxide (TiO_2) NPs (Tiwari et al., 2018). The TiO_2 nanoparticles, which had an average diameter of 280 nm, allowed for the control of lasing emissions by induced bending movements and supplied the extra scattering needed for random lasing (Tiwari et al., 2018). The absence of these nanoparticles would prevent the LCE from generating the required scattering (Tiwari et al., 2018). In a similar vein, researchers studied an LCRL using a dye-doped LC with a negative phase and cadmium sulphide nanoparticles (CdS) NPs (5 nm) for scattering (Li, 2017). The study reported that the threshold pump energy needed for lasing was dramatically reduced when the concentration of CdS NPs was increased from 0.026 g to 0.12 g. The nanoparticles are responsible for the improvement in gain and scattering, as reported in (Li, 2017).

3.3 Quantum dots as gain medium in PDLC random lasers

A study in 2020 showed that the combination of a nematic liquid crystal (E7) and ZnCdSeS/ZnS quantum dots in a PDLC structure produces a low-threshold and stable random laser (Wang Z. et al., 2020) (Figure 9). The LC droplets act as a scattering core, while the QDs provide optical gain. The optimized preparation procedure resulted in a random laser with a low threshold of 50 μJ/cm^2 and very good stability, retaining 92% of the initial emission intensity after 3 h of daily excitation for 2 weeks.

3.4 Soliton effect random lasers

A soliton is a self-reinforcing solitary wave that maintains its form while moving at a steady speed. Solitons form from a careful balance of nonlinear and dispersive processes in the medium through which they travel. For waveguided LCRLs using the soliton effect, an optical pump power is needed for excitation, and near-infrared (NIR) light is needed to confine and guide the produced random laser emission (Perumbilavil et al., 2018a). The NIR laser can reorient the liquid crystal molecules, producing the waveguiding action. When exposed to an electric field, for example, through a light beam, the rod-shaped molecules of nematic liquid crystals reorient, resulting in a notable nonlinear optical response (Perumbilavil et al., 2018a). This response can reorient the molecules of the medium and alter the refractive index, causing the mesogens to align themselves along the direction of the electric field vector of the NIR laser beam. A nematicon is a spatial soliton in nematic liquid crystals, formed through the light-induced reorientation of the molecular director (Perumbilavil et al., 2018a). It balances two opposing effects, self-focusing and diffraction, to waveguide the light. The propagation of the nematicon with respect to the wave vector occurs at an angle called the walk-off angle. External stimuli, including magnetic and electric fields, can modify this angle by directing the NLC molecules, which in turn changes the nematicon's path. The random laser emission is one example of a light signal that this soliton can direct (Perumbilavil et al., 2018a).

Recently, several studies have demonstrated waveguided random lasers by externally stimulating the solitons via magnetic or electric fields. Using solitons to shape and guide the emission is an innovative way to overcome the drawbacks of random lasers,

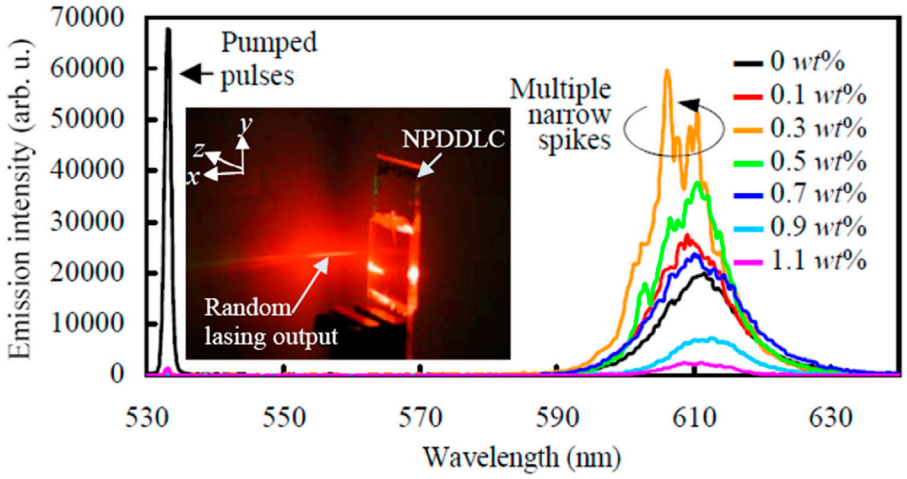

FIGURE 8
Demonstration of the random lasing enhancement after $BaTiO_3$ NPs at fixed pump power at 10 μJ/pulse. The optimal concentration is 0.3 wt%. (Reprinted with permission from (Lee et al., 2015) © Optical Society of America).

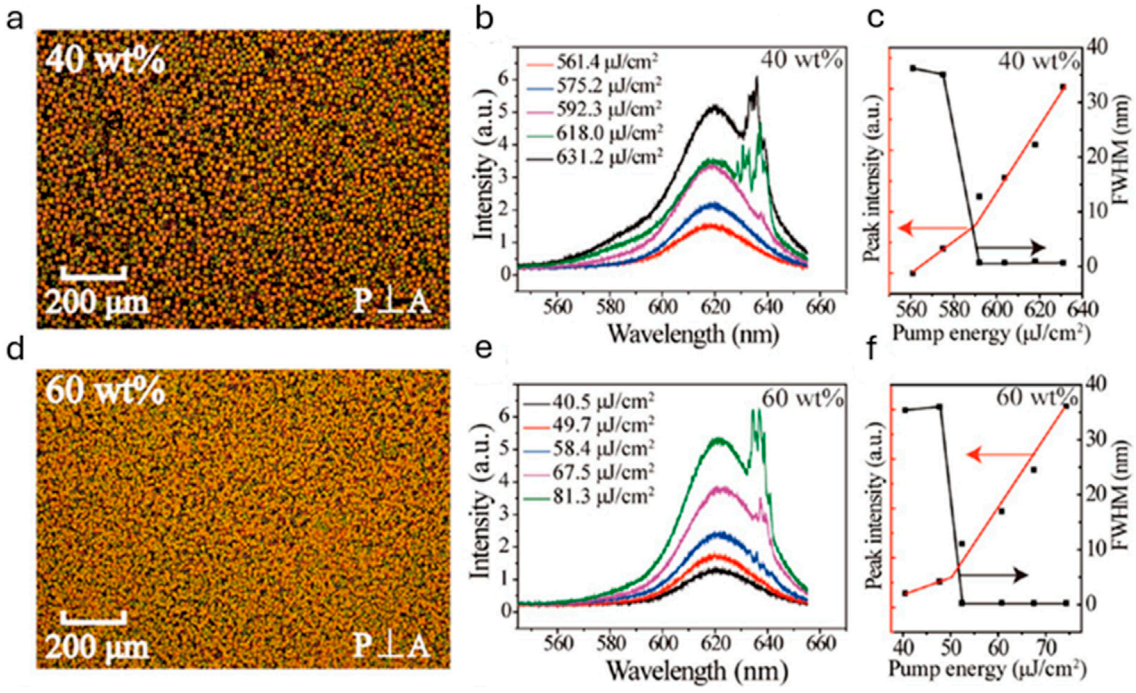

FIGURE 9
PDLC random lasers based on quantum dot gain medium at two concentrations. **(A-C)** for a 40 wt% concentration of QDs, which shows a much higher threshold than the optimal concentration **(D-F)** which is 60 wt% (Wang Z. et al., 2020). (Reproduced with permission from (Wang Z. et al., 2020) © 2020 American Chemical Society).

such as low beam quality and random emission direction, as can be seen in Figure 10A (Perumbilavil et al., 2018b). Practically, this can be accomplished by optically pumping the dye, which is dispersed in the liquid crystal, while applying a near-infrared nematicon beam. The solitons serve as a waveguide, containing and directing the random lasing emission. Consequently, the random laser emission shows improved directionality, a smoother beam profile, higher conversion efficiency from the pump to the laser output, the ability to turn on/off the control of the laser by the low-energy nematicon beam, and the capability to steer the laser beam path using external fields that move the nematicon (Perumbilavil et al., 2018b).

Similarly, by applying an external voltage, it is possible to steer an optically pumped dye-doped nematic liquid crystal random laser in a

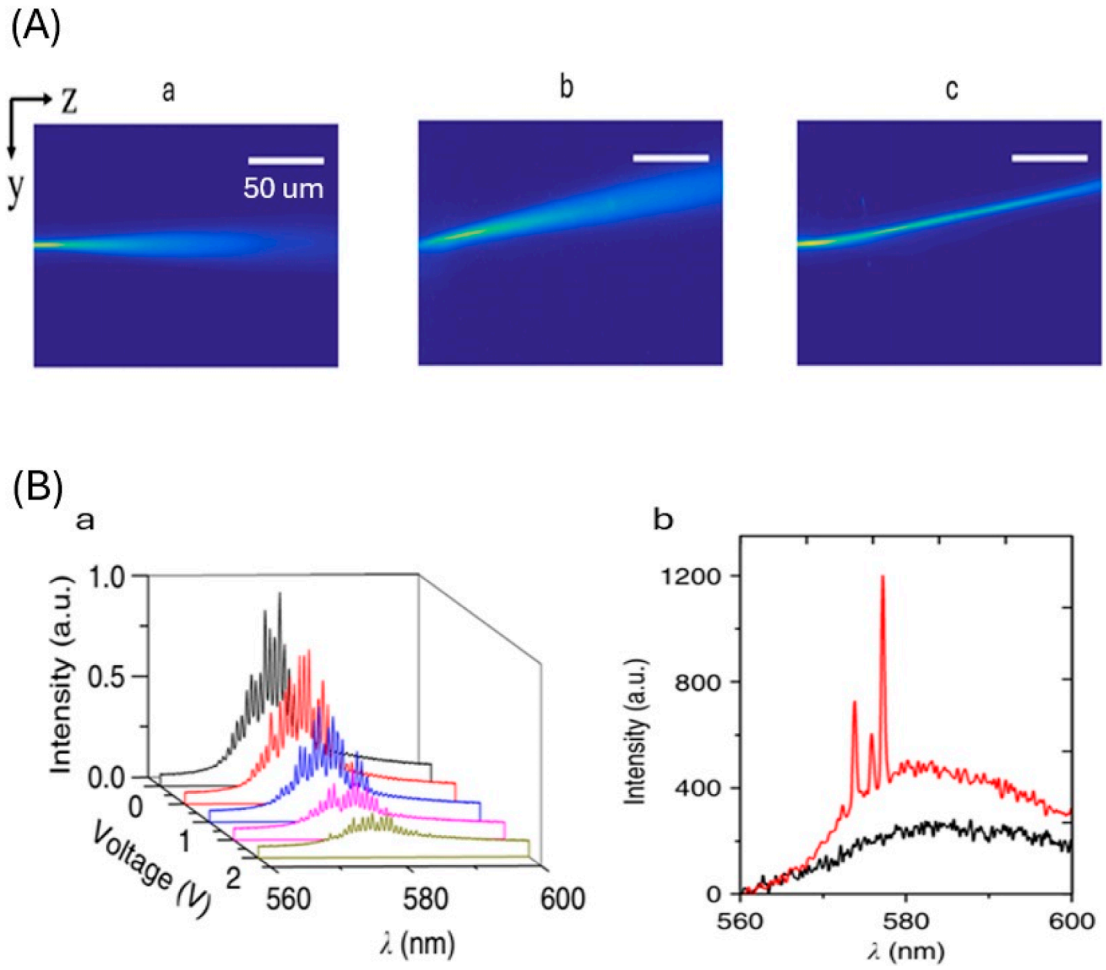

FIGURE 10
(A) Illustration of the waveguiding of random laser emission by solitons through NIR (1.064 μm) and external voltage application (Perumbilavil et al., 2018b). **(A)** Using ordinary-wave beam diffraction. **(B)** Extraordinary-wave NIR beam diffraction by applying low power NIR (0.7 mW) with walk-off propagation. **(C)** Extraordinary-wave beam by applying high-power NIR (5 mW) and self-confined into a nematicon with walk-off propagation. (Figure reprinted with permission from (Perumbilavil et al., 2018b) © Optical Society of America). **(B)** Effect of volt change on RL emission; and **(B)** with NIR input (6 mW, red line) and without NIR input (0 mW, black line) the random laser is observed to be switched on and off at a threshold energy of 0.45 μJ (Perumbilavil et al., 2018d). (licensed under CC BY).

specific angular orientation (Assanto et al., 2018). A near-infrared (NIR) spatial soliton, which functions as an all-optical waveguide to capture and direct the emitted light, is altered by this externally applied voltage. The random laser beam can be swept across a 7-degree angle by reducing the soliton's walk-off angle via altering the applied voltage between 0 and 2 V (Perumbilavil et al., 2018c). Moreover, the introduction of near-infrared (NIR) light at 6 mW and pulse energies of 0.55 μJ was found to enhance the random laser (RL) emission by focusing and concentrating the output at a specific bright spot (Perumbilavil et al., 2018c). In contrast, without the introduction of NIR light and with the same pulse energy, the emission remains random and distributed. The bright spot indicates the exit position of the nematicon, which is caused by the walk-off δ in the positive uniaxial medium (Perumbilavil et al., 2018c).

By applying an external magnetic field, a study showed in-plane angular steering of a green-pumped random laser using dye-doped nematic liquid crystals (Perumbilavil et al., 2018a). Here, a near-infrared reorientation spatial soliton yields a smooth output profile with emission in a well-defined direction. The angle of the soliton-guided random laser beam was steered up to 14° by changing the direction of the magnetic fields. Another important study that explored the influence of solitons on RL emission was reported in ref. (Perumbilavil et al., 2018d). The soliton was created using NIR light on NLCs to waveguide the RL emissions. As illustrated in Figure 10B part (b), varying the NIR input intensity allows the random laser to be switched on (red curve) and off (black curve), displaying transistor-like behaviour. When nematic liquid crystal random lasers are assisted by negations, an applied voltage can be utilized to adjust the direction and spatial profile of the laser emission (Perumbilavil et al., 2018d). The nematicon's walk-off angle, which is the angle between the Poynting vector and the soliton's wave vector, varies depending on the supplied voltage. By modulating the voltage, the walk-off angle can be reduced or tuned, thereby steering the direction of the output laser light (Perumbilavil et al., 2018d). As illustrated in Figure 10B part (a), the emission intensity of the

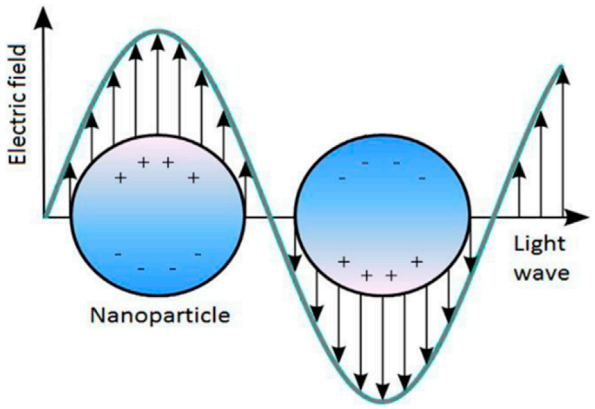

FIGURE 11
Schematic illustration of localized surface plasmon resonance (LSPR) on a metallic nanoparticle surface (Unser et al., 2015). (Figure reproduced from (Unser et al., 2015), licensed under CC BY 4.0).

random laser is controlled by varying the external voltage applied across the NLC cell (Perumbilavil et al., 2018d).

Although the presence of a soliton has no major effect on the lasing threshold, it does significantly enhance the lasing efficiency because the emission spectra become narrower (Perumbilavil et al., 2017). Combining solitons and random lasing in NLCs improves control over RL emission parameters, opening the path for future photonic applications (Perumbilavil et al., 2019).

3.5 Localized surface plasmon resonance and random lasers

Localized Surface Plasmon Resonance (LSPR) is an optical phenomenon that occurs when light interacts with metallic nanoparticles, such as gold or silver, which have a smaller size than the incident wavelength of light, as shown in Figure 11 (Unser et al., 2015). The interaction causes the conduction electrons on the nanoparticle's surface to vibrate collectively in response to the electric field vector of light (Unser et al., 2015).

In terms of the LSPR mechanism, when light irradiates a metallic nanoparticle, the oscillating electric field leads the conduction electrons to oscillate coherently. The entire oscillation is referred to as a localized surface plasmon. Furthermore, the resonance requirements are fulfilled when the incoming light frequency is equal to the natural frequency of electron oscillations. This causes a considerable amplification of the local electromagnetic field around the nanoparticle's surface. There are several factors influencing LSPR, such as changes in the size, shape, and conductivity of the nanoparticles, as well as changes in the dielectric environment of these nanoparticles. LSPR has many applications, including biosensors, spectroscopy, medical diagnostics, and lasers (Unser et al., 2015).

Recently, the effect of localized surface plasmon resonance on liquid crystal random lasers has been studied. Two dye doped polymer-stabilized liquid crystal random lasers (DDPSLC RLs) were developed by independently doping with silver (Ag) and zinc oxide (ZnO) nanoparticles (Chen et al., 2018). Doping with Ag NPs at a concentration of 0.1% by weight reduced the lasing threshold from 23.2 μJ/pulse to 10.9 μJ/pulse (Chen et al., 2018). At a 1% concentration of ZnO NPs, the lasing threshold was reduced to 21.2 μJ/pulse (Chen et al., 2018). As a consequence, the addition of Ag NPs increased the random lasing capabilities due to the improved scattering effect generated by localized surface plasmon resonance (LSPR) (Chen et al., 2018). Similarly, a study achieved a lower threshold energy of about 1.7 μJ/pulse due to LSPR by adding Ag NP at very low concentrations (Ye et al., 2016). By inserting and electrically manipulating Ag nanoparticles into dye-doped liquid crystal (DDLC) within the gaps of photonic crystal fibres, PCFs (Figure 12), a random laser with significantly improved performance was created by taking advantage of the localized surface plasmon resonance, resulting in greater light scattering and better lasing properties compared to a sample without Ag NPs (Xie et al., 2022).

In addition, gold nanorods, pyrromethene 597 (PM597, "donor"), and Nile blue (NB, "acceptor") were doped into chiral liquid crystals to achieve low-threshold and wide-range thermally tuneable random lasing (Qu G. Y. et al., 2023). This was achieved by combining the phenomenon of Förster resonance energy transfer (FRET) with surface plasmon resonance. Before the gold nanorods (GNRs) were added, the red lasing was not significant because PM597 and NB had a low FRET efficiency (Qu G. Y. et al., 2023). However, by incorporating GNRs into these random laser devices and taking advantage of their localized surface plasmon resonance effect, the FRET efficiency increased by 68.9%, lowering the lasing threshold. The longitudinal LSPR was tuned to match the NB emission wavelength, resulting in a 200 times increase in lasing intensity (Qu G. Y. et al., 2023) (Figure 13A).

Another noble metal nanoparticle material, platinum nanoparticles (Pt NPs), has proven to enhance random laser action by raising the spontaneous emission rate of laser dyes via local surface plasmon resonance (Wang et al., 2016). Pt NPs were added to dye-doped polymer-dispersed liquid crystals (DDPDLCs) to improve the random laser performance. It was reported that adding 1.0% Pt NPs reduced the threshold from 17.5 μJ/pulse to 8.7 μJ/pulse (Wang et al., 2016). An additional study has dispersed 40 nm-sized titanium nitride (TiN) nanoparticles into dye-doped nematic liquid crystals to design random lasers (Wan and Deng, 2020). The plasmonic effect was obtained through optical pumping. When TiN is present, the lasing threshold is 0.2 mJ/cm^2, while in the absence of TiN it is an order of magnitude larger, 2.0 mJ/cm^2 (Wan and Deng, 2020). Similar to gold and silver, TiN has plasmonic capabilities; however, it is less expensive and has greater thermal stability (Wan and Deng, 2020). A similar study on a DDNLC RL with added two types of nanoparticles: titanium dioxide (TiO_2) and titanium nitride (TiN) nanoparticles was carried out in ref. (Dai et al., 2020). TiO_2 nanoparticles are semiconductors, but TiN nanoparticles are metallic and show localized surface plasmon resonance (LSPR) comparable to gold nanoparticles. Because of the TiN plasmonic characteristics and greater scattering capabilities, it considerably lowered the random laser threshold to 5.11 μJ/pulse (Wan et al., 2022).

Referring to Figure 13B, a flexible random laser was developed using a dye-doped stretchable polymer film containing

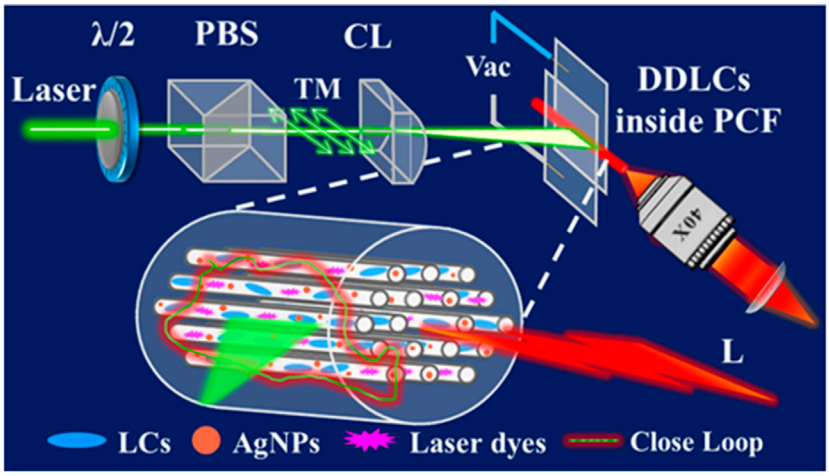

FIGURE 12
Schematic representation of the experiment setup for dye-doped liquid crystal (DDLC) within photonic crystal fibres (PCFs) with Ag NPs. (At the bottom, recurrent light scattering between holes inside the PCFs filling of NLCs) (Xie et al., 2022). (With permission from Elsevier).

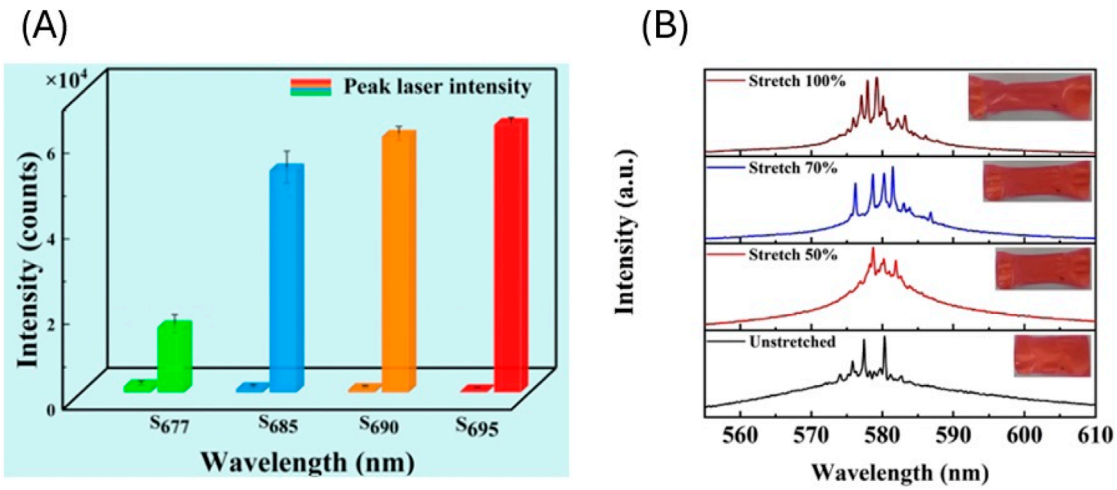

FIGURE 13
(A) Strength of the cholesteric liquid crystal random lasing (CLC) intensity before and after adding gold nanorods (GNRs) at different temperatures (Qu G. Y. et al., 2023). (Figure reproduced from (Qu G. Y. et al., 2023) under CC BY). **(B)** Intensity of a flexible random laser using a gold nanoparticle doped stretchable polymer film (elastomer)at varying strain (Dai et al., 2020). (Figure reproduced from (Dai et al., 2020) under CC BY).

nematic liquid crystals (NLCs) and gold nanoparticles with a diameter of 25 nm (Dai et al., 2020).

Due to the surface plasmon resonance effect, the films containing Au exhibited a low lasing threshold of approximately 0.62 mJ/cm^2, whereas no lasing was observed in films without Au even at a high pump energy of 16 mJ/cm^2. The laser's emission properties can be tuned by mechanically stretching the film.

Besides liquid crystal random lasers with their modifications through nanoparticles, quantum dots, negations and localized surface plasmon resonance, another recent approach with high application potential are liquid crystal white lasers and whispering gallery mode lasers, discussed in the following sections.

4 LC White lasers

Recently, white laser systems based on liquid crystal have emerged as a novel approach in the field of laser technology. This is particularly interesting because of its potential to emit white light by combining multiple wavelengths across the visible spectrum, such as red, green, and blue (RGB) (Szukalska and Mysliwiec, 2023) (Figure 14). This system uses the properties of liquid crystals, as well as advanced laser physics, to create a laser capable of producing white light. This section will cover such systems' methodologies, applications, and recent research.

Beside the classical Fabry-Perot resonator, there are three advanced resonator technologies that have recently been used

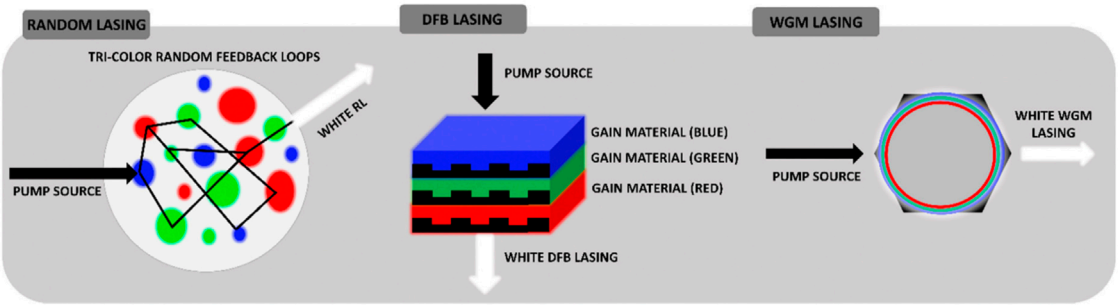

FIGURE 14
LC white lasers are based on three main physical phenomena, random scattering, distributed feedback (DFB),and Whispering Gallery Mode (WGM) (Szukalska and Mysliwiec, 2023). (Figure reproduced from (Szukalska and Mysliwiec, 2023) under CC BY).

in white laser production, namely, random distributed scattering (RDS), distributed feedback (DFB), and Whispering Gallery Mode (WGM) as summarised in Figure 14 (Szukalska and Mysliwiec, 2023). Nanoparticles, aggregates, crystals, liquid crystals, and droplets can all serve as randomly distributed scatterers (Szukalska and Mysliwiec, 2023).

Regarding the gain medium, one approach involves generating diverse wavelengths using liquid crystals doped with several laser dyes that emit different monochromatic colours (RGB: red, green, and blue). These are then combined to produce white light. Another option involves doping the LC with phosphor, which emits different wavelengths, then exciting it with a single wavelength laser and combining the emitted light to produce a white laser. A third approach uses broadband photoluminescent materials within the LC structure, where the liquid crystal helps to disperse light across a wide spectrum effectively. Examples of broadband photoluminescent materials include quantum dots (QDs), rare earth-doped materials, perovskite materials, and carbon dots.

In these systems, liquid crystals play a significant role in controlling and tuning the output light, for example, by modifying the orientation and therefore refractive index of the liquid crystal phase. The uniformity and quality of the white light produced can be improved by controlling the dispersion and combination of various wavelengths. Additionally, LCs can serve as waveguides or host matrices where the combination of light occurs. This guarantees the production of white light by effectively combining individual spectral components. However, the practical challenges that LC white laser systems impose are critical. One of the major challenges is the necessity of a precise control over the emitted light spectrum. This involves precisely controlling the intensity and bandwidth to achieve equilibrium among individual wavelength components to produce pure white light. Furthermore, the design of the LC matrix and the choice of appropriate dyes directly affect the effectiveness and thermal stability of the laser output. As temperature increases with high laser intensity output, thermal management is required to limit the heat effect on the alignment and possibly even the phase of the LC material.

In 2016, a spectrally discrete white-light laser device based on photonic band gap (PBG) hybrid structure was developed (Huang et al., 2016). This hybrid consists of a dye-doped cholesteric liquid crystal inserted between two imperfect but identical inorganic multilayer photonic crystals (Figure 15). The hybrid device can produce single, dual, or triple wavelength laser emissions when pumped by a single optical source. It generates three distinct spectral peaks: one from the photonic defect modes in dual-mode lasing, and two from the band edges of the CLC reflection band. This hybrid device offers electrical tunability in laser wavelength since the CLC pitch facilitates manipulation through applied voltages (Huang et al., 2016). Further, the CLC exhibits optical stability among planar, focal conic, and homeotropic states, allowing the lasing to alternate among band edge-mode, dual-mode, and defect-mode emissions. A discrete white-light laser was designed (see Figures 15A–C) with red, green, and blue emissions by carefully modifying the photonic crystal structure and dye composition (Huang et al., 2016). This organo-inorganic hybrid technique surpasses earlier organic and inorganic white laser sources in terms of cost-efficiency, manufacturing ease, and colour tuning.

A novel organic white laser device based on multiphase optical media containing liquid crystalline emulsions was designed in 2020 (Adamow et al., 2020) (Figures 15D,E). The active material of the white laser is composed of hydrophilic polyvinyl alcohol (PVA) with blue dye (SB420) and hydrophobic droplets of E7 nematic liquid crystal (NLC) with either red dye (DCM) or green dye (CM540). This material is placed in a glass cell. As can be seen in Figures 15D, E, by exciting a combination of different dyes (DCM, CM540, SB420), each corresponding to an RGB colour, doped in a polymer matrix of LC droplets at a threshold of around 12 mJ/cm^2, they accomplished both single-color and multi-colour laser emissions in the visible range. The intensity of the white laser can be adjusted by applying voltages up to 10 V.

The LC white laser systems are at the forefront of laser technology as they combine complex material science and optical fabrication. This is a rapidly advancing field of research that may lead to significant applications benefiting from these laser systems in the coming years, such as illumination, display technology, and optical communication.

5 Whispering gallery mode lasers

It is important to highlight the characteristics of the laser based on the whispering gallery mode (WGM) resonator, as it is utilized

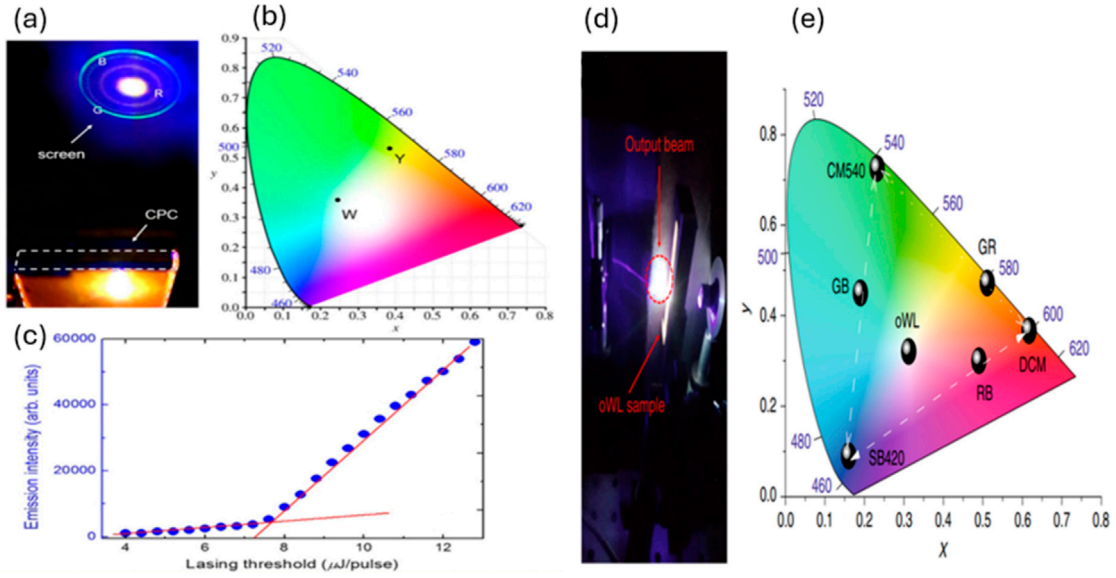

FIGURE 15
Illustration of the two LC white lasers. **(A-C)** A hybrid white laser consists of a dye-doped cholesteric liquid crystal placed between two identical dielectric mirrors (Huang et al., 2016). Both the mirrors and the CLC share the same one-dimensional bandgap, allowing them to be coupled effectively. White light lasing was achieved by the combination of three dyes (C540A, PM580 and LD688) (Huang et al., 2016). (Figure reproduced from (Huang et al., 2016) under CC BY). **(D-E)** show white LC lasing accomplished by three dyes (DCM, CM540, SB420) which are red, green, and blue, respectively (Adamow et al., 2020). The blue dye is mixed with PVA, while the red and green dyes are mixed with E7 to form droplets. All of these components are then placed together in a glass cell (Adamow et al., 2020). (Figure reproduced from (Adamow et al., 2020) under CC BY).

in a cholesteric liquid crystal (LC) material that exhibits photonic band gap (PBG) properties (Wang et al., 2021). This integration enhances optical functionalities due to the PBG's selective reflection coupled with the high Q-factor of WGM resonators. The WGM lasing occurs in a spherical microdroplet, an ideal shape that supports WGM resonances through its spherical cavity geometry and significant refractive index contrast with the surrounding medium. Additionally, the spectral range of the laser should align well with the calculated free spectral range (FSR) for the resonator, described by $\Delta\lambda = \lambda^2/n\pi D$, where λ is the laser wavelength, n is the effective refractive index, and D is the diameter of the droplet. The FSR, $\Delta\lambda$, determines the spacing in wavelength between sequential resonant modes in a cavity, ensuring the best resonator performance (Wang et al., 2021).

In order to create lasers based on the whispering gallery mode (WGM), a noteworthy report used three distinct laser dyes and chiral dopants, altering their concentrations in a matrix of LC host material within microdroplets injected into fibres, (see Figure 16) (Wang et al., 2021). Throughout the visible spectrum, it was possible to precisely manipulate unique lasing wavelengths and colours. Included in this were lasing techniques with adjustable colour temperatures that were monochrome, dual-, tri-, and white-coloured (Wang et al., 2021).

Another important study developed a whispering gallery mode (WGM) laser by filling a hollow optical fibre (HOF) with a dye-doped nematic liquid crystal (NLC) (E7) (Zhu et al., 2023). As demonstrated in Figure 18A, part of the HOF was sandwiched by ITO glass and by applying external electric fields and adjusting the temperature, the LC's refractive index and light scattering characteristics were altered, which allowed for more precise adjustments of the laser emission wavelength. Emissions were combined from various locations by applying patterned voltages and adjusting the pump position, which exhibited stability and repeatability under voltage control. Patterned voltages refer to the intentional and controlled application of voltage in specific spatial patterns to achieve desired effects in various electrical and photonic devices. In modern materials and electronics, patterned voltages are crucial, as the spatial distribution of voltage can significantly impact system performance and functionality. This research lays the groundwork for spectrally programmable soft-material lasers (Zhu et al., 2023).

Similarly, a rectangular fibre without tapering allows some energy to penetrate to the edge of the microsphere, exciting both the PBG mode and the WGMs (Zhou et al., 2023). As a result, a novel, non-invasive detection method for organic vapours and gases was developed. This method, based on the tapered fibre shape, effectively suppresses the WGM laser and produces a powerful single-mode PBG laser peak.

Likewise, by using scattering-assisted liquid crystal micropillar fibres, a new kind of whispering gallery mode was designed (Zhang et al., 2022). This improved light coupling and made self-seeding and self-guiding possible, which improved the performance of WGM lasers (Zhang et al., 2022).

In addition, the construction of an erasable read-write liquid memory device is made possible by the special characteristics of the liquid crystal, which are impacted by thermal forces (Zhang et al., 2022). For instance, electrically aligning the LC molecules in the micropillar structure by using an AC voltage. Moreover, when the temperature changes, thermal forces induce the LC molecules to reorient. Nevertheless, because of the viscous intermolecular

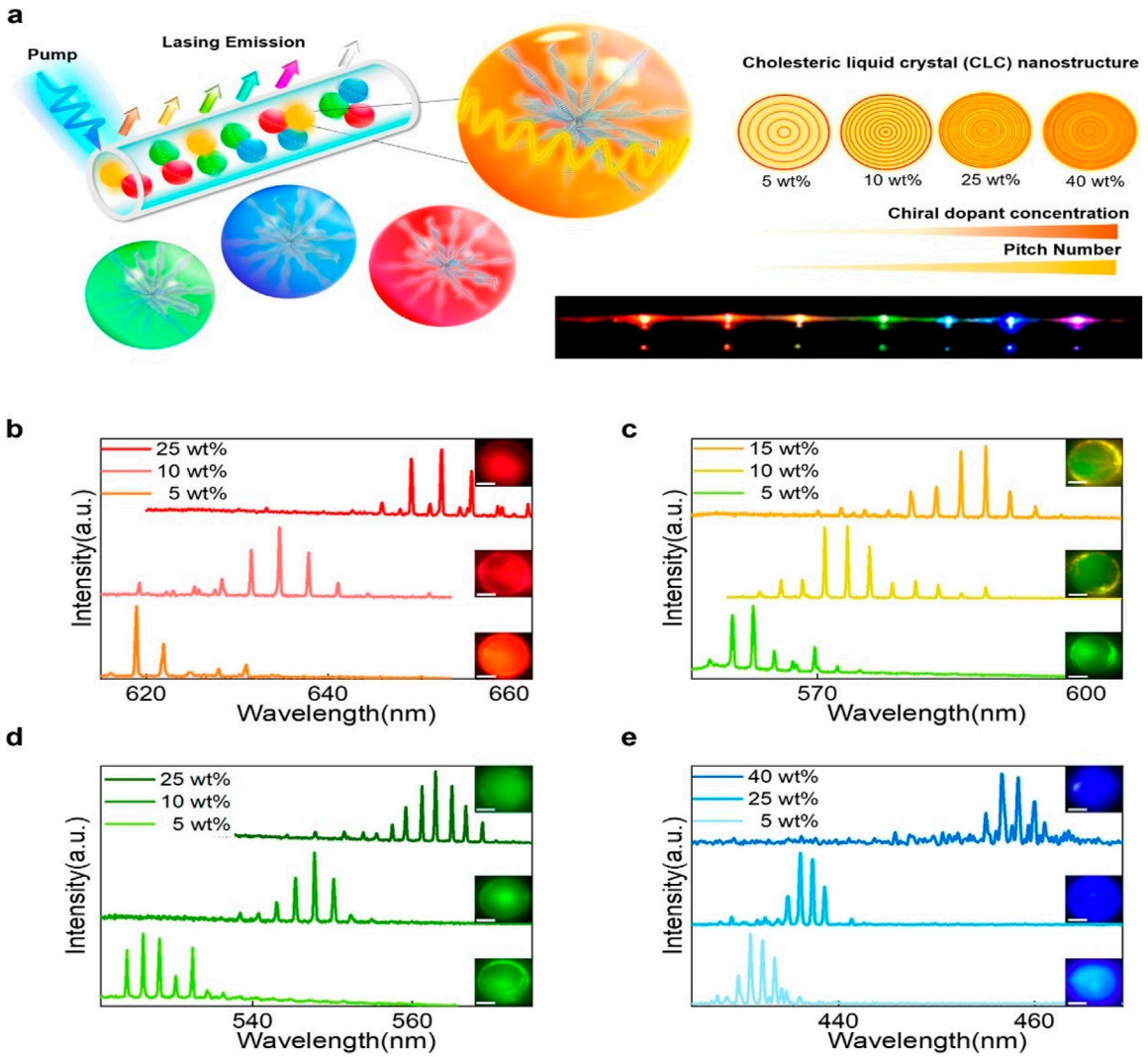

FIGURE 16
(A) A schematic representation of an optofluidic fibre filled with multicoloured cholesteric liquid crystal (CLC) microdroplets, each generating a different laser wavelength. The nanoscale topological structures of the CLC droplets were shifted by changing the concentrations of the chiral dopant (5, 10, 25, and 40 wt%), yielding pitch numbers of 5, 9, 23, and 37, respectively. A rainbow-coloured optofluidic fibre laser operating at 355 nm is shown in the bottom right corner. The fibre has a diameter of around 142 μm. **(B–E)** Lasing spectra of dye-doped CLC droplets with various chiral dopant concentrations **(B)** NR-doped CLC droplets with chiral dopant concentrations of 5, 10, and 25 wt%; **(C)** B2-doped CLC droplets with chiral dopant concentrations of 5, 10, and 15 wt%; **(D)** B1-doped CLC droplets with chiral dopant concentrations of 5, 10, and 25 wt%; **(E)** o-MSB-doped CLC droplets with chiral dopant concentrations of 5, 25, and 40 wt%. The excitation wavelength is 355 nm. Insets show CCD pictures of photoluminescence from the respective CLC lasing droplets. All the droplet dimensions were adjusted to 26 ± 1 μm (scale bar 10 μm) (Wang et al., 2021). (Reprinted with permission from (Wang et al., 2021). Copyright 2021 American Chemical Society).

interactions, they display a "memory effect" or hysteresis, tending to keep their prior orientation until the thermal force is sufficiently high. This bistable behaviour allows the LC molecules to exist in two distinct orientation states at the same temperature, depending on their previous state, allowing for logical operations such as "0" and "1" states. One can change between these states in a reconfigurable and erasable way by adjusting the voltage and temperature (Zhang et al., 2022). Fundamentally, the capacity of electrically anchored LC molecules to display hysteresis and bistability under temperature allows for logical memory and control functions in the proposed WGM laser apparatus. This novel proposal creates new opportunities for the use of logic controllable WGM lasers in optical control and storage applications (Zhang et al., 2022).

In addition, a thermally tuned whispering gallery mode (WGM) micro-laser using dye-doped cholesteric liquid crystal (CLC) microdroplets was developed (see Figure 18B) (Zhao et al., 2017). It offers optimal reversibility and excellent spectral quality, making it well-suited for temperature-sensing applications in liquids or integrated electronics, as shown in Figure 17.

Another micro-shell device was created by covering silica-glass microspheres with dye-doped cholesteric liquid crystals, as illustrated in Figure 18C (Lu Y. L. et al., 2018). Photonic band gap (PBG) and whispering gallery mode (WGM) lasers were observed separately by altering the chiral agent concentration and the pumping energy. Although the wavelength of the whispering-gallery modes (WGMs) laser can be tuned by changing the

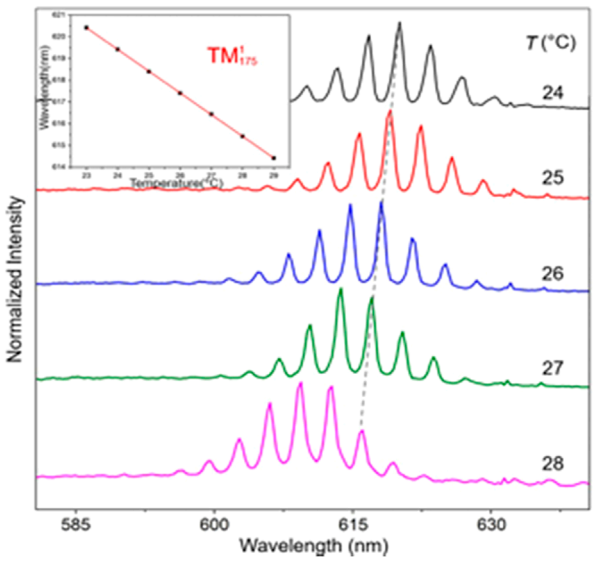

FIGURE 17
Temperature dependence of the lasing spectrum of a CLC microdroplet. There is a clear linear relationship between temperature and wavelength tuning as demonstrated in the inset (Lu Y. L. et al., 2018). (Reprinted from (Zhao et al., 2017),with permission from Elsevier).

diameter, both characteristics can be adjusted by altering the temperature (Lu Y. L. et al., 2018).

A comparative study developed three laser modes from exclusively dye-doped cholesteric liquid crystals, which are distributed feedback (DFB), distributed Bragg reflector (DBR) (or it can be referred to Fabry-Perot (FB)), and whispering gallery (WG) modes, by varying the pumping beam diameter (Lin Y.-L. et al., 2017). It was discovered that a small beam diameter exclusively excites the DFB mode at the photonic band gap (PBG). However, as the beam diameter increased, the DBR and WG modes were competitively activated, subsequently suppressing the DFB mode (Lin Y.-L. et al., 2017). Moreover, the lasing spectra for DDCLC micro-shells were measured with varying beam diameters (Lin Y.-L. et al., 2017). At a small diameter of approximately 1.2 mm, only distributed feedback (DFB) laser emission was observed around 593 nm. When the beam diameter increased to 4.5 mm, three types of lasers were detected: DFB at 593 nm, Fabry-Perot (FP) at 584 nm, and Whispering Gallery Mode (WGM) laser at 623 nm. At a larger diameter of approximately 8.6 mm, only FP and WGM lasers were detected at 584 nm and 623 nm, respectively. Regarding the lasing threshold, the threshold for DFB increased with the beam diameter, while the thresholds for FP and WGM decreased (Lin Y.-L. et al., 2017).

A further study fabricated a three-dimensional DBR microcavity laser that consists of three layers, which are a DDCLC microdroplet, polyglycerol-2 (PG2), and a hollow glass microsphere (HGM) (Hu et al., 2019). This laser is thermally and electrically tuneable and can be switch electrically from PBG and WGM modes to exclusively WGM mode at higher electric fields (Hu et al., 2019). Regarding the electrical sensitivity of the laser, when the LC microdroplet laser is made of electrically sensitive materials, any change in the charge distribution affects the internal configuration of the LC droplet's director field, which in turn influences the laser output (Wang Z. Y. H. et al., 2020). A bio-electrostatic, responsive LC microdroplet laser was fabricated, which was based on a WGM resonator for the ultrasensitive detection of negatively charged biomolecules (Wang Z. Y. H. et al., 2020). It was observed that the WGM laser wavelength shifts because of the binding of negative and positive charges, causing a reorientation of molecules from radial to bipolar configurations.

Another method for fabricating WGM lasers was designed based on soap bubbles made of amphiphilic molecules (soap), water, glycerol, fluorescein sodium salt and a dye-doped smectic liquid crystal bubble, as shown in Figures 19A–D (Korenjak and Humar, 2024). Through manipulation of these bubbles, it was possible to adjust the lasing emission's wavelength, as shown in Figures 19B, D (Korenjak and Humar, 2024).

With a consistent molecular thickness down to a single layer, smectic bubbles have been proven to be more stable than soap bubbles. This allows for stable, tuneable single-mode lasing sources with emission spectra resembling a comb of frequencies (Figure 19D) (Korenjak and Humar, 2024).

A study explored the emission of laser vector beams from liquid crystal superstructures with topological defects in a Fabry-Pérot (FP) microcavity (Papič et al., 2021). This microcavity is made up of two closely spaced dichroic mirrors that may generate structured light with specified intensity and polarisation characteristics (Papič et al., 2021). This cavity arrangement achieves more focused light emission, compared to the omnidirectional emission characteristic of whispering gallery mode (WGM). The work emphasises the importance of the FP microcavity in stabilising laser modes and producing coherent light with well-defined polarisation and intensity profiles (Papič et al., 2021). The authors employed the nematic phase of 5CB and added dyes such as Nile Red, Pyrromethene 580, and Rhodamine B, as well as the CB15 chiral dopant (Papič et al., 2021). The chiral dopant was employed to initiate a cholesteric phase, resulting in torons and chiral fingers that were subsequently used in the experiment (Papič et al., 2021). The work also demonstrated the emission of laser vector beams (VBs) with various polarisation profiles from these liquid crystal (LC) superstructures. The laser's polarisation features include radial, azimuthal, hybrid, and linear polarisation (Papič et al., 2021). These polarisation states were obtained by varying the orientation of the LC molecules and dye molecules within the LC structures, resulting in complicated vector beams with specific polarisation profiles (Papič et al., 2021).

In the following we discuss some further developments which are more materials related, through the derivation of liquid crystal-based materials for innovative lasers from biological structures and macromolecules.

6 Bio-derived liquid crystal materials for laser innovations

Liquid crystal materials exhibit a variety of phase structures, each characterized by distinct morphological and molecular arrangements. These structures are also prevalent in biological systems in various forms. For example, some beetles exhibit a

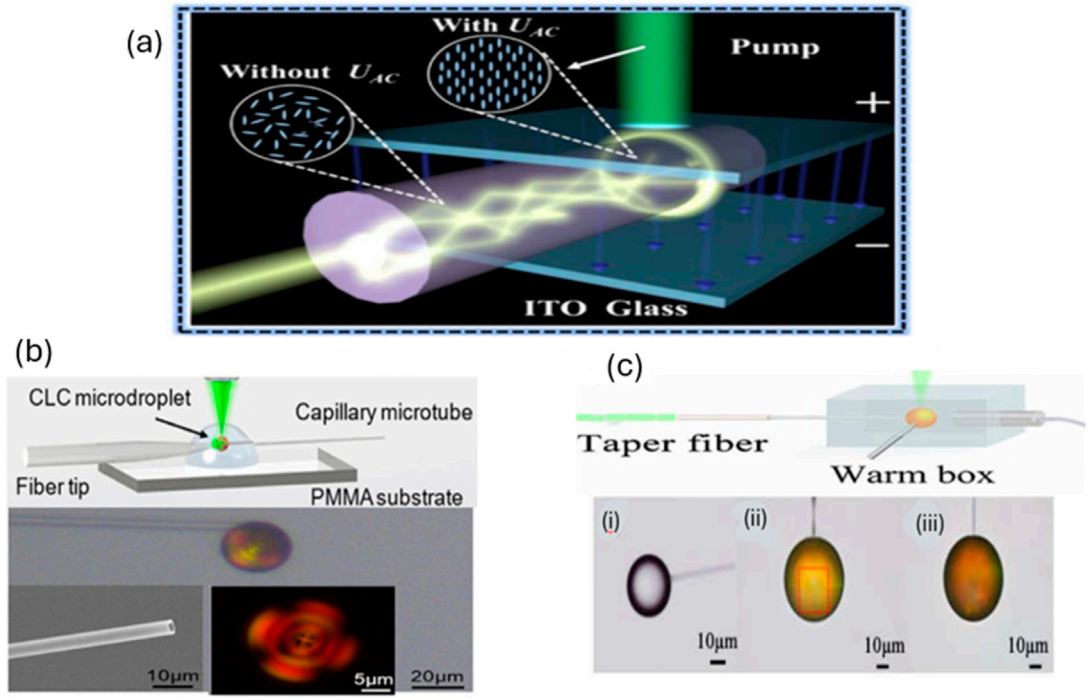

FIGURE 18
schematic outline of the different WGM RLs. **(A)** show the hollo optical fibre (Zhu et al., 2023) (Reprinted from (Zhu et al., 2023), with permission from Elsevier). **(B)** CLC microdroplet (Zhao et al., 2017) (Reprinted from (Zhao et al., 2017), with permission from Elsevier). **(C)** (i) silica-glass microspheres; (ii) partially coated DDCLC micro-shells; and (iii) fully coated DDCLC micro-shells (Lu Y. L. et al., 2018). (Reproduced from (Lu Y. L. et al., 2018). © 2018 by the authors. Licensed under CC BY).

polymerized cholesteric-like, helical structure of their outer shell, while the wings of butterflies display a nematic or smectic-like order. Furthermore, the cholesteric phase can be synthesized by casting cellulose nanocrystal suspensions at low concentrations, ranging from 2% to 10% and forming a lyotropic LC phase. These environmentally friendly and bio-based LC phases found in nature hold significant promise for future applications in fields such as lasing, sensing, and advanced optical devices. Recent advancements in lasing applications utilizing LC phases observed in living organisms have been demonstrated.

6.1 Nematic phase random laser in butterfly wing

A successfully developed liquid crystal random laser using butterfly wings, which exhibit a natural nematic phase (Shang et al., 2023) was demonstrated in 2023 (Figure 20). This integration greatly improves the stability of laser emissions. The results indicate that the microstructures of butterfly wings have an important role in increasing the performance of bio-random lasers (Shang et al., 2023).

In this study, three different samples were prepared: 4-(Dicyanomethylene)-2-methyl-6-(4-dimethylaminostyryl)-4H-pyran (DCM) laser dye with LC, DCM laser dye with LC and butterfly wing, and Pyrromethene 597 (PM597) laser dye with butterfly wing. The lasing thresholds for these samples were found to be 69.9 μJ, 183 μJ, and 161 μJ, respectively (Shang et al., 2023). Although the wing structure improved the emission stability and reduced spectrum spikes, it did not consistently lower the lasing threshold as compared to the non-biological liquid crystal random laser system. The wing structure helped to localize the optical field and varied the emission patterns, which improved stability at the cost of increasing the lasing threshold (Shang et al., 2023). Nonetheless, for reducing the lasing threshold, pumping at an angle of 0° instead of 90° has been shown to be successful. Additionally, incorporating metallic nanoparticles, which are known for their threshold-reducing properties due to surface plasmon resonance (SPR) effects, could be considered in future research.

6.2 Cholesteric cellulose nanocrystal-based laser

Cellulose nanocrystals (CNCs) are exciting candidates for green and sustainable nanotechnology devices (Lagerwall and Scalia, 2016). Their attractive optical and mechanical properties make them suitable for various applications, such as smart windows and tuneable lasers. CNCs are an essential organic polymer with the general formula $(C_8H_{10}O_5)_n$ (Figure 21) (Banerjee et al., 2020). They have a spindle-like shape and can be found in wood (around 45%) and cotton (around 90%) (Lagerwall and Scalia, 2016). Moreover, some bacteria can produce up to 90% pure CNCs to form a bio-CNC film (Lagerwall and Scalia, 2016).

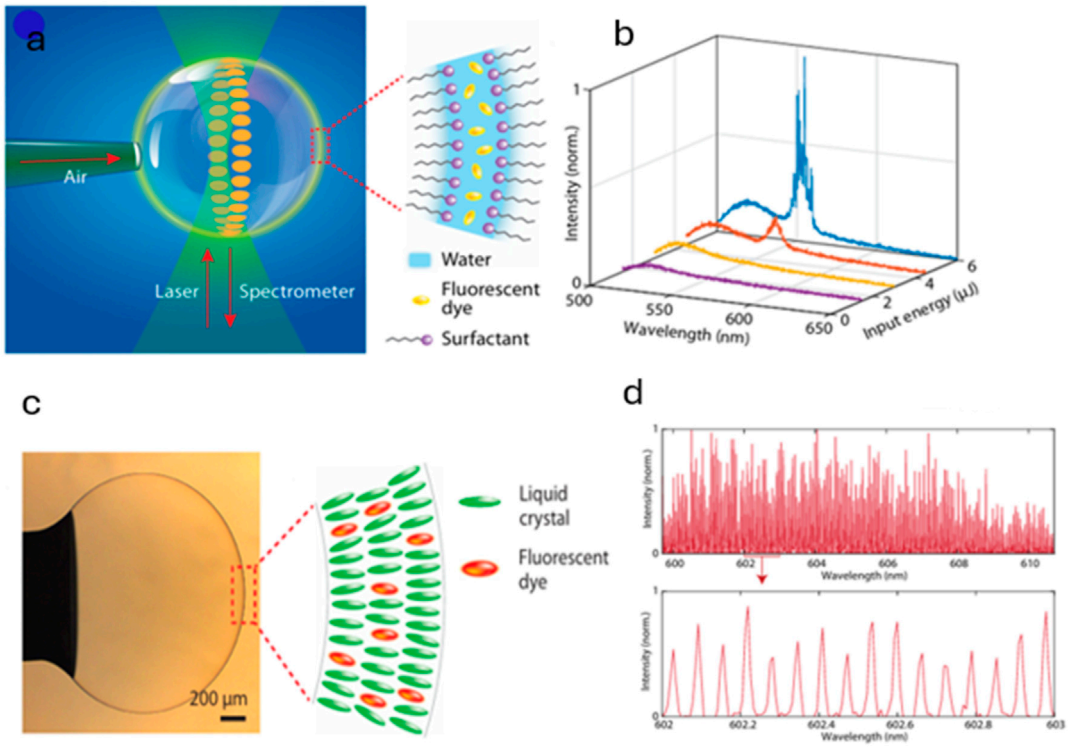

FIGURE 19
WGM laser based on soup and smectic bubbles. **(A)** A schematic diagram of the experimental setup with a dye-doped soap bubble being inflated at the end of a horizontal capillary and irradiated with a laser from below. The soap film is comprised of layers of surfactant molecules mediated by water and fluorescent dye molecules. **(B)** Spectrum transmitted by a soap bubble connected to the end of a capillary as the pump laser's pulse energy increases. At low energy levels, luminescence is observed, while at higher pump energies, distinct lasing peaks develop. **(C)** An experimental smectic bubble of diameter 1.75 mm, with the diagram illustrating the film's molecular structure. **(D)** The Lasing spectrum over a broad range of wavelengths (top curve, 600–610 nm) has a frequency comb shape when viewed at magnification (bottom curve, 602–603 nm) (Korenjak and Humar, 2024). (Reprinted from (Korenjak and Humar, 2024), licensed under CC BY 4.0).

CNCs have a range of beneficial characteristics, including a high melting point of around 467°C, high mechanical strength, optical transparency, birefringence, low weight, and a low thermal expansion coefficient (Lagerwall and Scalia, 2016). They are hydrophilic and indissoluble in water or other solvents, but it can be suspended in water (Lagerwall and Scalia, 2016).

There are several techniques for preparing a CNC suspension, but many of the stages are comparable (Lagerwall and Scalia, 2016). One such approach is to extract cellulose nanocrystals (CNCs) with sulphuric acid and cotton (Lagerwall and Scalia, 2016). To obtain high crystallinity and particular nanostructures, a series of crucial procedures are required. It starts with the processing of cotton fibres, which are washed and possibly bleached to eliminate contaminants. The cotton is then acid hydrolysed by being treated with 64% sulphuric acid at a temperature of 45–50°C. This process is critical because it degrades the amorphous sections of cellulose, leaving behind crystalline nanorods. After the acid hydrolysis is completed, the process is stopped by diluting the liquid with water. The suspension is then filtered and carefully washed to eliminate any remaining acid. Centrifugation is then used to remove big particles, purify the CNCs, and accomplish size fractionation, which improves the consistency and stability of the CNC suspension. Following this, the CNC suspension is dialysed against water for several days to neutralise the pH and remove any remaining acid. Sonication is an option for improving the CNCs' dispersion and stability (Lagerwall et al., 2014).

One of the most advantageous features of the CNC suspension in water is its ability to form a lyotropic cholesteric liquid crystal phase at concentrations below 10% (Lagerwall et al., 2014). When the CNC suspension is cast on a glass slide, it naturally forms a left-handed helical structure (Lagerwall et al., 2014). The solid photonic crystal film selectively reflects light in the visible range after the evaporation of the water. The pitch, and therefore the photonic band gap (PBG), of cellulose nanocrystal films can be adjusted using a variety of methods, including ultrasonic treatment in suspension (Duan et al., 2022), polymer addition (such as polyethylene glycol (PEG)) (Duan et al., 2022) and carboxylation (Fan et al., 2022), concentration and thickness adjustment (Wei et al., 2023), electrolyte addition (such as NaCl) (Zhao et al., 2022), salt intercalation (Guo et al., 2020), self-assembly, and environmental conditions (Tao et al., 2021). Each of these approaches influences the films' structural colour and optical characteristics. This tuning capability is critical for applications involving photonic devices, sensors, and lasers (Lagerwall et al., 2014).

Recently, some research groups have exploited the CNC cholesteric structure and developed circularly polarized lasers

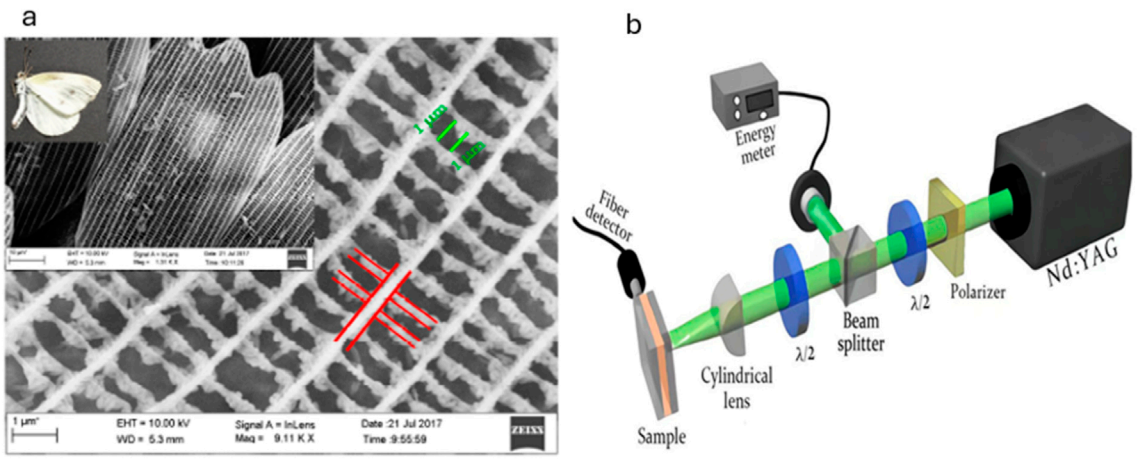

FIGURE 20
A nematic random laser based on a butterfly wing. **(A)** shows the full image and SEM images of the *Pieris Rapae Crucivora* butterfly wing. **(B)** Schematic diagram of the experimental setup (Shang et al., 2023). (Reprinted from (Shang et al., 2023), licensed under CC BY 4.0).

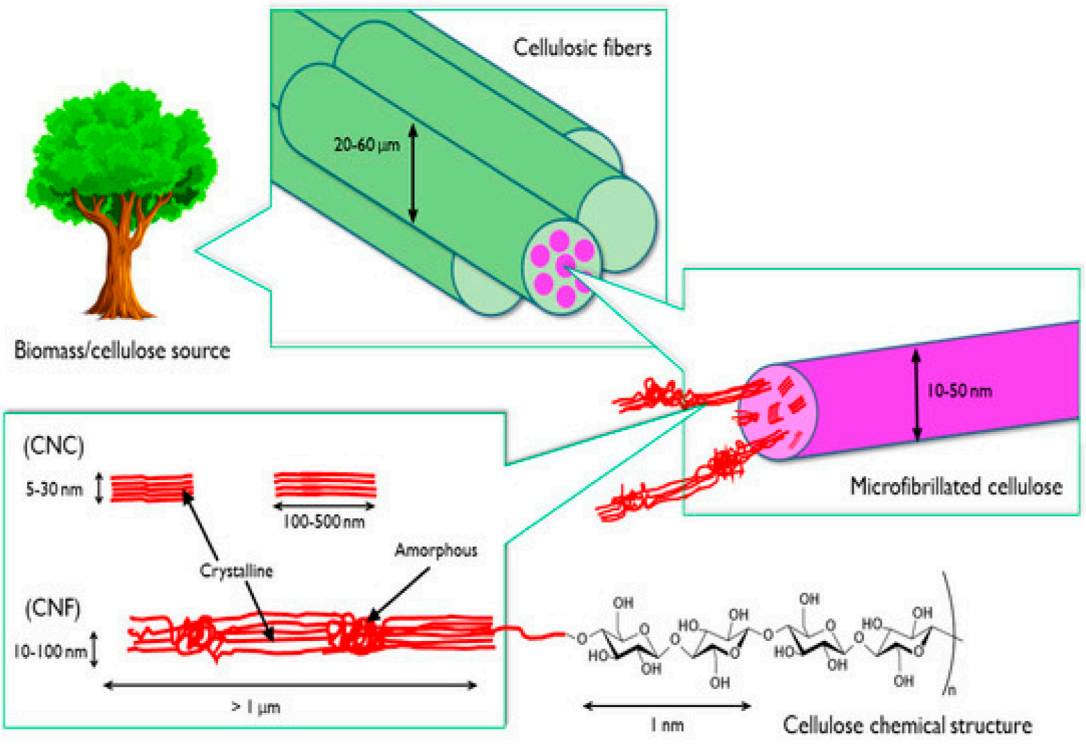

FIGURE 21
Diagram illustrating the hierarchical structure of nanocellulose. It shows the source (tree), cellulosic fiber (diameter 20–60 µm), microfibrillated cellulose (diameter 10–50 nm), cellulose chemical structure, cellulose nanofiber (CNF) (diameter 10–100 nm), and cellulose nanocrystal (CNC) (diameter 5–30 nm) (Banerjee et al., 2020). (Figure reproduced from (Banerjee et al., 2020), licensed under CC BY 4.0).

(Guo et al., 2020; Qu et al., 2021). Employing a CNC suspension doped with the Rhodamine B laser dye, casting the solution to produce thin films, and facilitating CNC lasers was demonstrated. Rhodamine B's photoluminescence wavelength is 600 nm, and the laser was pulsed at 545 nm, slightly below the maximum absorption wavelength, to obtain a reduced lasing threshold (Guo et al., 2020). The photonic band gap (PBG) was modified by varying the CNC to poly (ethylene glycol-co-hydroxyethyl methacrylate) (poly (EG-co-HEMA)) ratio, which was chosen to overlap with Rhodamine B's emission spectrum at roughly 600 nm (Guo et al., 2020). At 33% humidity, the lasing threshold of the CNC/poly (EG-co-HEMA Rho) film is 7.2 mJ cm^{-2}. Although the asymmetry factor

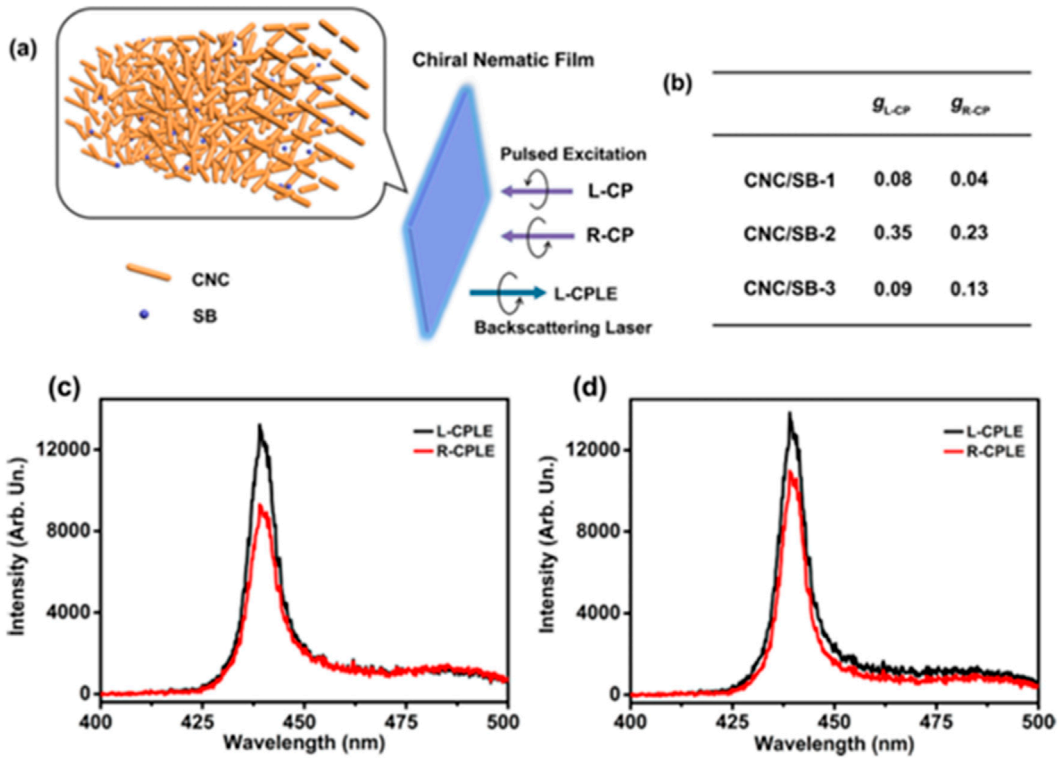

FIGURE 22
(A) Diagram of CNC-based CPLE: The overlap between the photonic band gap (PBG) of the left-handed chiral nematic CNC/SB film and the luminescence of the stilbene 420 dye enables L-CPLE to be activated by L-CP or R-CP laser light. **(B)** A comparison of the dissymmetry factors g_L-CP with L-CP laser excitation and g_R-CP with R-CP laser excitation. The CNC/SB-2 film exhibits L-CPLE and R-CPLE spectra after excitation (fluence = 90 mJ cm^{-2}) with **(C)** L-CP and **(D)** R-CP lasers, with L-CPLE being the primary component (Qu et al., 2021). (Reprinted from (Qu et al., 2021), licensed under CC BY-NC-ND 4.0. © 2021 American Chemical Society).

is not expressly specified, the CNC's inherent left circular selective reflection shows polarisation asymmetry (Guo et al., 2020).

Lately, a thin-film circular polarised laser was successfully carried out by casting a CNC suspension containing the stilbene 420 (SB) laser dye (Qu et al., 2021). Three samples with different wavelengths of selective reflection were produced, which were tuned by ultrasonication, as illustrated in Figure 22. The sample with a 425 nm selective reflection wavelength performed better because it almost matched the dye's photoluminescent emission peak, which is 444 nm. The films were pumped with left circularly polarized (LCP) light, right circularly polarized (RCP) light, and linearly polarized separately (Qu et al., 2021).

When stimulated by LCP light, the films emitted a strong left circularly polarized laser emission (LCPLE) with a dissymmetry factor of up to 0.35 and a threshold of 13 mJ cm^{2}. This effect is attributable to the CNC's left-handed chirality (Qu et al., 2021).

6.3 DNA in liquid crystal lasers

Deoxyribonucleic acid (DNA) is a basic molecule that contains the genetic code for all living beings and many viruses (Zhang Y. et al., 2020; Brach et al., 2016; Camposeo et al., 2014; Chow et al., 2010). DNA exhibits a right-handed double helix made up of two complementary strands of nucleotides called adenine (A), thymine (T), cytosine (C), and guanine (G) (Chow et al., 2010). These nucleotides (A with T and C with G) produce the distinctive double helix shape *via* hydrogen bonding (Chow et al., 2010). Aside from its well-known role in genetics, DNA has unique physical characteristics that enable it to form liquid crystalline phases under specific circumstances (Zhang Y. et al., 2020; Brach et al., 2016; Camposeo et al., 2014; Chow et al., 2010). For instance, when DNA is dissolved in concentrated aqueous solutions, it can form liquid crystalline phases (Camposeo et al., 2014). The anisotropic shape of DNA molecules enables them to align in specified orientations, resulting in the development of organized structures (Brach et al., 2016). As can be seen in Figure 23, the texture of the cholesteric and columnar hexagonal of the DNA is observed due to its ability to self-assemble (Brach et al., 2016).

Liquid crystal phases exhibited in DNA have various possible applications due to their unique optical characteristics, which include birefringence and selective reflection (Mitov, 2017). These properties make them ideal for use in innovative materials and electronics, such as developing tuneable photonic liquid crystals, lasers, sensors, and other optoelectronic devices (Zhang Y. et al., 2020; Brach et al., 2016; Camposeo et al., 2014; Mitov, 2017).

LC DNA solution can be prepared by adding DNA to deionized water at relatively high concentrations, ranging from around 6% to 29 wt%. The solution is then ultrasonicated to obtain uniform sized DNA molecules of approximately 250–1000 base

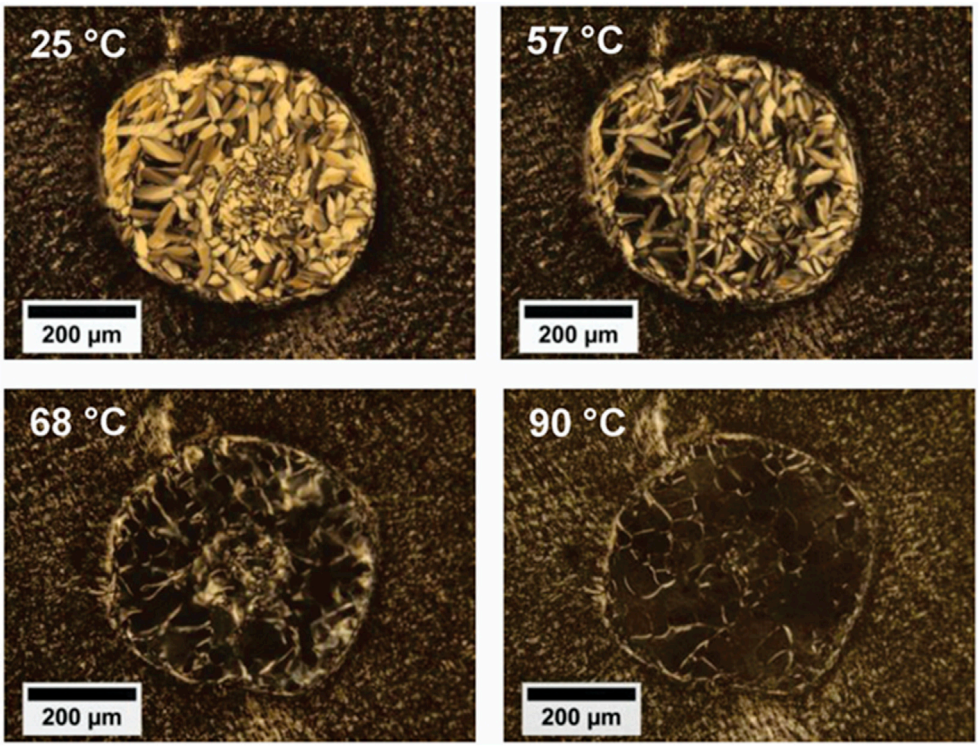

FIGURE 23
Textures of DNA lyotropic LC phases from 6% of DNA. By increasing the temperature, the gold NR-doped DNA LC cell stabilizes the phases. (a) At 25°C, a columnar hexagonal texture is shown. (d) At 90°C, a cholesteric phase is observed (Brach et al., 2016). (Figure reprinted from (Brach et al., 2016), © 2021, American Chemical Society, licensed under CC BY-NC-ND 4.0).

pairs (Brach et al., 2016; Chow et al., 2010). The role of DNA in LC lasers includes tuning the wavelength and forming lyotropic LC phases at high concentrations that can be used in lasing applications (Zhang Y. et al., 2020; Brach et al., 2016).

A recent study demonstrated a tuneable and reversible bio-laser that uses the bio-interface between single-stranded DNA (ssDNA) and complementary DNA (cDNA) in a dye-doped nematic liquid crystal (LC) mixture (5CB NLC, DCM dye, surfactant OTAB) within a Fabry-Perot microcavity (Zhang Y. et al., 2020). The surfactant octadecyl trimethyl ammonium bromide (OTAB) coating on liquid crystal surfaces supports homeotropic alignment (Zhang Y. et al., 2020). This sensitive laser is accomplished by adding ssDNA to the NLC mixture at different concentrations, which binds to the surfactant layer (OTAB) surrounding the liquid crystals *via* electrostatic interactions (Zhang Y. et al., 2020). This binding causes the liquid crystal molecules to shift from a perpendicular to a flat orientation (Zhang Y. et al., 2020). As a result, the DCM dye molecules in the LC mixture change their absorption characteristics, causing the laser wavelength to shift towards blue. When cDNA is added after ssDNA at different concentrations, it hybridizes with the ssDNA already bound to the liquid crystal interface, resulting in double-stranded DNA (dsDNA) (Zhang Y. et al., 2020). This creation disturbs the DNA-liquid crystal connection, causing the LC molecules to revert to their original perpendicular orientation (Zhang Y. et al., 2020). As a result, the laser wavelength becomes redshifted and returns to its original value (Zhang Y. et al., 2020). This dynamic and reversible mechanism for tuning the laser emission wavelength represents a substantial development in the field of bio-lasers (Zhang Y. et al., 2020). Furthermore, this biologically adjusted lasing system opens new possibilities for the design of extremely sensitive and programmable photonic devices (Zhang Y. et al., 2020).

The following outlook may serve as a basis for discussion and possible directions that the field of lasing with liquid crystals might take in the near future.

7 Outlook

To begin with nanoparticles and their impact on liquid crystal lasers, their integration offers an appealing path for improving lasing efficiency, tunability, and beam control due to the unique interactions between nanoparticles and liquid crystal material. Exploring different nanoparticles and their combined effects within liquid crystals might open new possibilities for constructing improved laser systems with adjustable optical characteristics for specific applications. A current study demonstrates the effectiveness of Al_2O_3 (150 nm) particles in a polymer matrix for random lasing (Cao et al., 2018). Future research could explore integrating this and other nanoparticles into liquid crystal materials to enhance random laser performance, aiming for lower thresholds, increased scattering, and tuneable wavelengths. Within the visible range, the pitch length of photonic LC phases is approximately

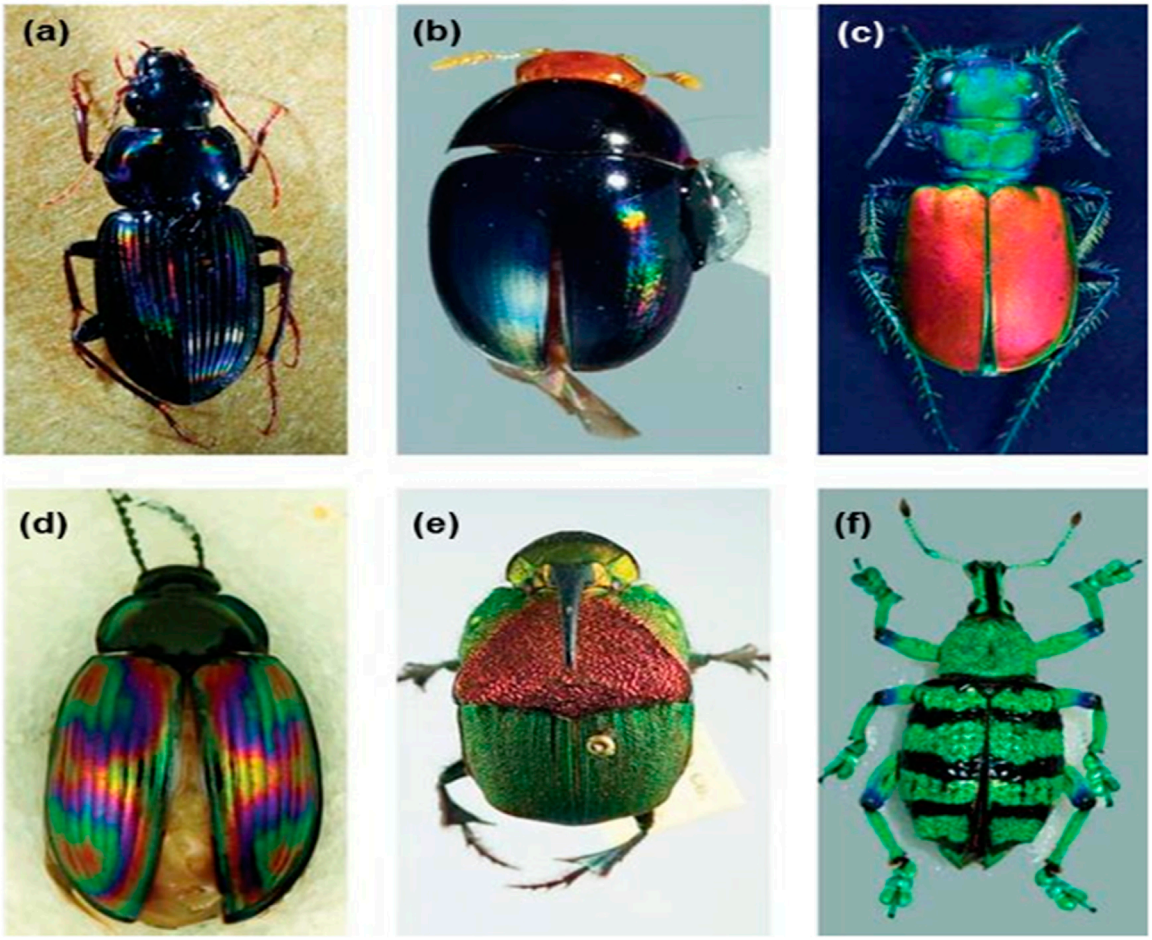

FIGURE 24
Various beetle species exhibiting iridescence: **(A)** *Loxandrus rectus* (Carabidae), **(B)** Phalacridae *gen. sp.*, **(C)** *Cicindela scutellaris scutellaris* (Carabidae), **(D)** *Amarygminae gen. sp.* (Tenebrionidae), **(E)** *Phanaeus vindex* (Scarabaeidae), and **(F)** *Eupholus* sp. (Curculionidae) (Seago et al., 2009). (Reproduced with permission from (Seago et al., 2009). Journal of The Royal Society Interface).

300 nm. Nanoparticles close to or larger than this pitch length may interfere with the photonic band gap (PBG) and introduce defects, thereby enabling random lasing in cholesteric phases while potentially increasing scattering and reducing thresholds. Investigating the impact of nanoparticles of varying sizes on scattering magnitude and lasing performance can provide further fundamental understanding of the influence of nanoparticles on lasing action. Moreover, exploring the addition of nanoparticles to different LC phases with photonic properties, such as blue phases, cholesteric phase, ferroelectric liquid crystals, chiral ferroelectric nematic phase, and possibly even twist grain boundary phases, could provide phase specific properties in addition to those of the dispersed nanoparticles for improved lasing performance. Specific nanoparticles such as quantum dots could be used as both a gain medium and a thermal stabilizer for LC phases, facilitating the fabrication of various lasers, including random lasers, band edge lasers (PBG phases), LC-DBR, LC-DFB, and whispering gallery mode (WGM) lasers. Additionally, using a combination of quantum dots (QDs) and nanoparticles (NPs) for LC laser design could be beneficial. QDs can act as the gain medium, while NPs serve as scatterers and thermal stabilizers. Incorporating polymers or the use of elastomers into these suggested systems may lead to optimal control in the manufacturing of LC lasing devices for various applications.

Beside lasing, whispering gallery mode (WGM) illumination plays a significant role in visualizing injected water nanodroplets, making them easier to track within the liquid crystal host drop (Guo J. K. et al., 2019). This advantage facilitated the fabrication and reconfiguration of complex double emulsions with hierarchical structures, consisting of water microdroplets dispersed within a liquid crystal host droplet (Guo J. K. et al., 2019). Although WGM lasers can be designed without liquid crystals, the dynamic tuning range is significantly limited compared to LC-based WGMs. For example, the RGB colour model and far-field photographs of the emitted light from integrated CQD lasers demonstrate that additive colours such as yellow, pink, and cyan, at certain percentages, can produce a white light laser. These colours are observed by selectively exciting two or three RGB CQD lasers, consistent with the principles of the RGB colour model (Chen et al., 2023). This field of research has successfully developed a WGM using a simple, surfactant-free approach to assemble colloidal quantum dots (CQDs) into high-quality whispering-gallery-mode lasers (Chen et al., 2023).

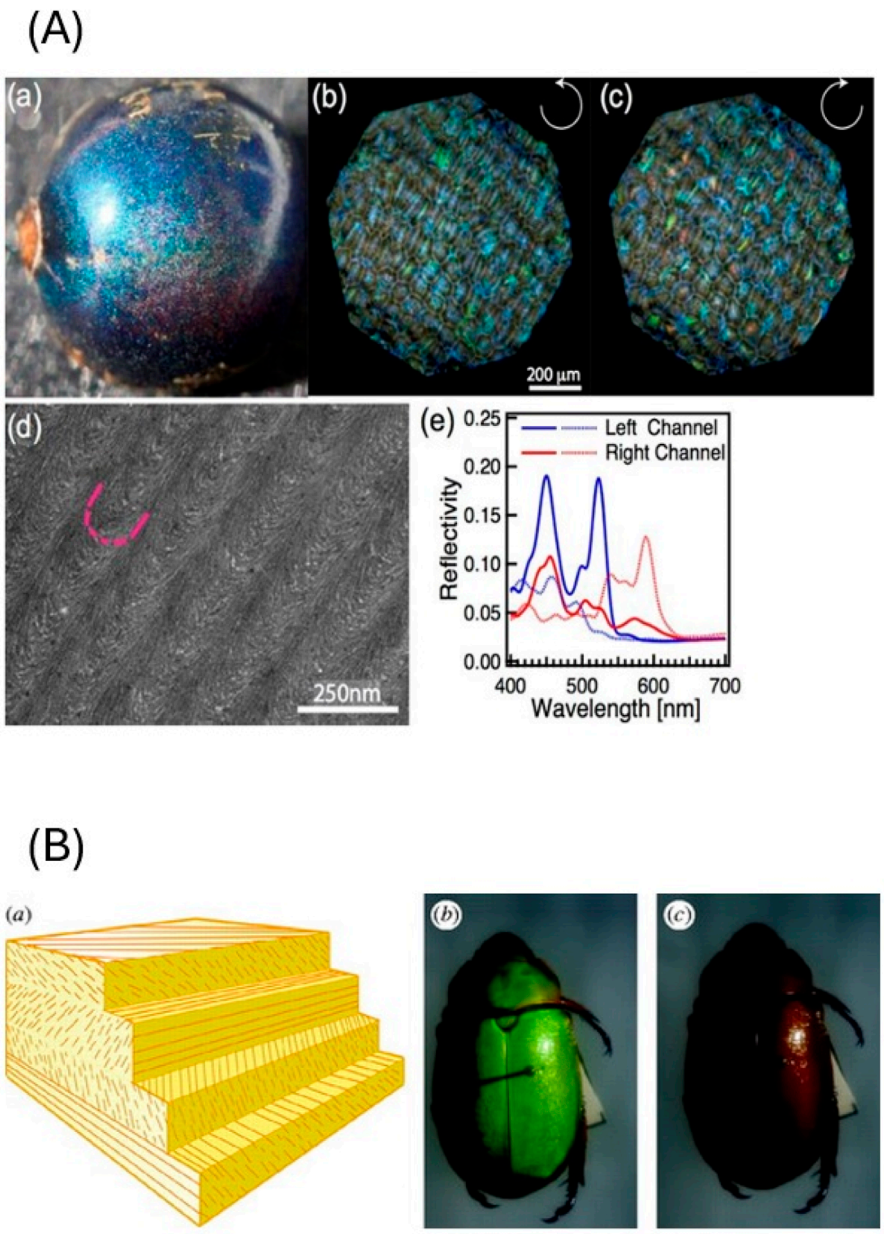

FIGURE 25
(A) (A) Image of a *Pollia condensata* fruit. **(B, C)** Microscopic images show the two circular polarization channels and the rich pointillistic colouring that originates from individual pigmented cells in the epicarp. **(D)** The features of the helicoidal pattern are present in the Bouligand cut TEM image of the epicarp (pi-twist of intrinsic helical twist is indicated by the red line). **(E)** Single-cell reflectivity spectra were collected at two different sites in the left (blue) and right (red) circular polarization channels (Wilts et al., 2014). (Reprinted with permission from (Wilts et al., 2014). © 2014 Elsevier). **(B)** Multilayered reflectors with a circular polarisation. **(A)** Schematic of helical multilayer reflector; **(B)** *Chrysina boucardi* observed *via* a quarter wave plate rotated 0°; **(C)** *Chrysina boucardi* photographed through a quarter wave plate turned 90° (Seago et al., 2009). (Reproduced with permission from (Seago et al., 2009). Journal of The Royal Society Interface).

These lasers offer static tuning across the entire visible spectrum by changing sizes or compositions. However, the range of dynamic tuning is relatively small, up to 4.7 nm, achieved by altering the surrounding refractive index (Chen et al., 2023). In the future, it will be possible to base these systems on liquid crystals, allowing easy and large range tuning and control of colour and dynamic emission. An additional way for developing tuneable photonic devices based on liquid crystal elastomers (LCEs) with whispering gallery mode resonators was created using 3D laser printing (Woska et al., 2020). It was found that the performance and functionalities of these tuneable photonic devices, which rely on stimulus-responsive LCEs, were enhanced by the incorporation of WGM (Woska et al., 2020). This enhancement is attributed to WGM's contributions, including high-quality factors, reversible tunability by changing the distance between two WGMs via heat, and enabling evanescent coupling in LCEs (Woska et al., 2020). While the major focus of the article in ref (Woska et al., 2020) is on WGM resonators, the techniques and materials presented might be useful for the creation

of random lasers, especially in terms of tunability, flexibility, and improved optical feedback. In terms of polarisation, liquid crystal (LC) materials are extremely versatile, allowing for the manipulation of a wide range of polarisation states in laser systems, such as linear, circular, radial, and azimuthal polarisation, among others. These materials provide fine control over the polarisation, phase, and spatial structure of laser beams through the use of custom-designed LC cells, spatial light modulators, or other LC-based optical components. This versatility makes LC materials important in sophisticated applications such as optics, telecommunications, quantum information, and material processing. The development of LC materials for creating multiple complicated polarisation states in lasers is a potential topic of study for the next years.

Future research may certainly explore the use of biomaterials (Figure 24) that exhibit liquid crystal-like structures for designing lasers based on random scattering, distributed Bragg reflector (DBR), distributed feedback (DFB), or whispering gallery mode (WGM) cavities.

Cholesteric structures, found in a wide variety of biological systems such as lyotropic liquid crystal phases, for example, from DNA, chromatin, cellulose, silk, bacteriophages, archaea, bone, tendon, cornea, cuttlebone, and squid pen, offer significant potential for photonic applications. Mitov has reviewed these examples (Mitov, 2017).

The cholesteric liquid crystals that generate the vibrant structural colours are an essential component of the exoskeleton cuticle, which encases the entire beetle body, including the rigid front wings (elytra) that cover and protect the flight wings when the beetle is not in flight. This enables the reflective colours to be exhibited over the beetle's entire body (Figure 24) (Seago et al., 2009; Scarangella et al., 2020; Agez et al., 2017; Sharma et al., 2014). Utilizing these beetle wings, or other parts that have LC phase structure, could be advantageous in dye lasers. By sandwiching the dye laser with beetle wings and ensuring that the selective reflection of the wings matches the dye emission, one can achieve the amplification conditions necessary for lasing when optically pumped. DNA has many liquid crystal properties, which can be used to develop novel biological devices. Moreover, adding gold nanorods has been proven to thermally stabilize the DNA LC phases and facilitate the observation of plasmon resonance phenomena (Brach et al., 2016). In addition to the stability provided by gold nanoparticles, this approach could be beneficial for making low-threshold bio-lasers by adding DNA-modified gold nanoparticles to dye lasers, due to the plasmon resonance effect.

Similarly, any biological material with a cholesteric structure could be used in lasing applications (Figures 24, 25). Lasing performance can be enhanced by leveraging other phenomena such as surface plasmon resonance (SPR) for threshold reduction and solitons for waveguide random lasers. Additionally, exploring fibre and microdroplet lasers with Whispering Gallery Mode (WGM) could provide further insights and advancements in this field.

Author contributions

OA: Writing–original draft, Writing–review and editing. ID: Conceptualization, Resources, Supervision, Writing–original draft, Writing–review and editing.

Funding

The author(s) declare that no financial support was received for the research, authorship, and/or publication of this article.

Conflict of interest

The authors declare that the research was conducted in the absence of any commercial or financial relationships that could be construed as a potential conflict of interest.

Publisher's note

References

Adamow, A., Szukalski, A., Sznitko, L., Persano, L., Pisignano, D., Camposeo, A., et al. (2020). Electrically controlled white laser emission through liquid crystal/polymer multiphases. *Light Sci. and Appl.* 9 (1), 19. doi:10.1038/s41377-020-0252-9

Agez, G., Bayon, C., and Mitov, M. (2017). Multiwavelength micromirrors in the cuticle of scarab beetle Chrysina gloriosa. *Acta biomater.* 48, 357–367. doi:10.1016/j.actbio.2016.11.033

Assanto, G., Perumbilavil, S., Piccardi, A., and Kauranen, M. (2018). Electro-optic steering of random laser emission in liquid crystals. *Photonics Lett. Pol.* 10 (4), 103–105. doi:10.4302/plp.v10i4.852

Azmi, A. N., Wan Ismail, W. Z., Abu Hassan, H., Halim, M. M., Zainal, N., Muskens, O. L., et al. (2022). Review of open cavity random lasers as laser-based sensors. *Acs Sensors* 7 (4), 914–928. doi:10.1021/acssensors.1c02749

Bagchi, K., Emeršič, T., Martínez-González, J. A., de Pablo, J. J., and Nealey, P. F. (2023). Functional soft materials from blue phase liquid crystals. *Sci. Adv.* 9 (30), eadh9393. doi:10.1126/sciadv.adh9393

Banerjee, M., Saraswatula, S., Williams, A., and Brettmann, B. (2020). Effect of purification methods on commercially available cellulose nanocrystal properties and TEMPO Oxidation. *Processes* 8 (6), 698. doi:10.3390/pr8060698

Berreman, D. W., and Scheffer, T. J. (1970). Bragg reflection of light from single-domain cholesteric liquid-crystal films. *Phys. Rev. Lett.* 25 (9), 902–581. doi:10.1103/physrevlett.25.902.4

Brach, K., Matczyszyn, K., Olesiak-Banska, J., Gordel, M., and Samoc, M. (2016). Stabilization of DNA liquid crystals on doping with gold nanorods. *Phys. Chem. Chem. Phys.* 18 (10), 7278–7283. doi:10.1039/c5cp07026k

Camposeo, A., Del Carro, P., Persano, L., Cyprych, K., Szukalski, A., Sznitko, L., et al. (2014). Physically transient photonics: random versus distributed feedback lasing based on nanoimprinted DNA. *ACS Nano* 8 (10), 10893–10898. doi:10.1021/nn504720b

Cao, D., Huang, D., Zhang, X., Zeng, S., Parbey, J., Liu, S., et al. (2018). Alumina particles doped in a polymer film act as scatterers for random laser generation. *Laser Phys.* 28 (2), 025801. doi:10.1088/1555-6611/aa914b

Cao, W., Muñoz, A., Palffy-Muhoray, P., and Taheri, B. (2002). Lasing in a three-dimensional photonic crystal of the liquid crystal blue phase II. *Nat. Mater* 1 (2), 111–113. doi:10.1038/nmat727

Castles, F., Day, F. V., Morris, S. M., Ko, D. H., Gardiner, D. J., Qasim, M. M., et al. (2012). Blue-phase templated fabrication of three-dimensional nanostructures for photonic applications. *Nat. Mater* 11 (7), 599–603. doi:10.1038/nmat3330

Chanishvili, A., Chilaya, G., Petriashvili, G., Barberi, R., Bartolino, R., Cipparrone, G., et al. (2004). Lasing in dye-doped cholesteric liquid crystals: two new tuning strategies. *Adv. Mater.* 16 (9-10), 791–795. doi:10.1002/adma.200306542

Chanishvili, A., Chilaya, G., Petriashvili, G., Barberi, R., Bartolino, R., Cipparrone, G., et al. (2005). Widely tunable ultraviolet-visible liquid crystal laser. *Appl. Phys. Lett.* 86 (5), 051107. doi:10.1063/1.1855405

Chen, C. W., Huang, H. P., Jau, H. C., Wang, C. Y., Wu, C. W., and Lin, T. H. (2017). Polarization-asymmetric bidirectional random laser emission from a twisted nematic liquid crystal. *J. Appl. Phys.* 121 (3). doi:10.1063/1.4974476

Chen, C.-W., Jau, H. C., Wang, C. T., Lee, C. H., Khoo, I. C., and Lin, T. H. (2012). Random lasing in blue phase liquid crystals. *Opt. Express* 20 (21), 23978–23984. doi:10.1364/oe.20.023978

Chen, C. W., Li, C. C., Jau, H. C., Yu, L. C., Hong, C. L., Guo, D. Y., et al. (2015). Electric field-driven shifting and expansion of photonic band gaps in 3D liquid photonic crystals. *ACS Photonics* 2 (11), 1524–1531. doi:10.1021/acsphotonics.5b00314

Chen, M. Z., Dai Hai-tao, 戴., Luo Dan, 罗. 丹., Zhang Xiao-dong, 张., and Liu Chang-long, 刘. (2018). Properties of random laser based on polymer stabilized liquid crystal doped with nanoparticles. *Chin. J. Liq. Cryst. Displays* 33 (1), 14–22. doi:10.3788/yjyxs20183301.0014

Chen, W. G., Wang, L., Liu, R., Shen, H., Du, J., and Fan, F. (2023). Self-Assembled and wavelength-tunable quantum dot whispering-gallery-mode lasers for backlight displays. *Nano Lett.* 23 (2), 437–443. doi:10.1021/acs.nanolett.2c03409

Chow, M. H., Yan, K. T. H., Bennett, M. J., and Wong, J. T. Y. (2010). Birefringence and DNA condensation of liquid crystalline chromosomes. *Eukaryot. cell* 9 (10), 1577–1587. doi:10.1128/ec.00026-10

Coles, H., and Morris, S. (2010). Liquid-crystal lasers. *Nat. Photonics* 4 (10), 676–685. doi:10.1038/nphoton.2010.184

Dai, G., Wang, L., and Deng, L. G. (2020). Flexible random laser from dye doped stretchable polymer film containing nematic liquid crystal. *Opt. Mater. Express* 10 (1), 68–75. doi:10.1364/ome.10.000068

de Vries, H. (1951). Rotatory power and other optical properties of certain liquid crystals. *Acta Crystallogr.* 4 (3), 219–226. doi:10.1107/s0365110x51000751

Dierking, I. (2014). Chiral liquid crystals: structures, phases, effects. *Symmetry* 6 (2), 444–472. doi:10.3390/sym6020444

Dreher, R., Meier, G., and Saupe, A. (2007). Selective reflection by cholesteric liquid crystals. *Mol. Cryst. Liq. Cryst.* 13 (1), 17–26. doi:10.1080/15421407108083534

Duan, R., Lu, M., Tang, R., Guo, Y., and Zhao, D. (2022). Structural color controllable humidity response chiral nematic cellulose nanocrystalline film. *Biosensors* 12 (9), 707. doi:10.3390/bios12090707

Fan, W., Wang, Z., Yu, X., Li, J., and Xu, Y. (2022). Carboxylated cellulose nanocrystals for depolarization films. *ACS Appl. Polym. Mater.* 4 (5), 3811–3819. doi:10.1021/acsapm.2c00276

Finkelmann, H., Kim, S. T., Muñoz, A., Palffy-Muhoray, P., and Taheri, B. (2001). Tunable mirrorless lasing in cholesteric liquid crystalline elastomers. *Adv. Mater.* 13 (14), 1069–1072. doi:10.1002/1521-4095(200107)13:14<1069::aid-adma1069>3.0.co;2-6

Folcia, C. L., Ortega, J., Sierra, T., Martínez-Bueno, A., and Etxebarria, J. (2024). *Chiral ferroelectric nematic liquid crystals as materials for versatile laser devices*. arXiv preprint arXiv:2402.12420.

Ford, A. D., Morris, S. M., Pivnenko, M. N., and Coles, H. J. (2004). "A comparison of photonic band edge lasing in the chiral nematic N ∗ and smectic C ∗ phases," in *Liquid crystal materials, devices, and applications X and projection displays X* (SPIE), 5289, 213–220.

Ford, A. D., Morris, S. M., and Coles, H. J. (2006). Photonics and lasing in liquid crystals. *Mater. Today* 9 (7-8), 36–42. doi:10.1016/s1369-7021(06)71574-7

Furumi, S., and Tamaoki, N. (2010). Glass-forming cholesteric liquid crystal oligomers for new tunable solid-state laser. *Adv. Mater* 22 (8), 886–891. doi:10.1002/adma.200902552

Goldberg, L., and Schnur, J. (1973). Tunable internal-feedback liquid crystal-dye laser. *U.S. Pat*.

Goodby, J. W. (2012). Twisted and frustrated states of matter. *Proc. R. Soc. A Math. Phys. Eng. Sci.* 468 (2142), 1521–1542. doi:10.1098/rspa.2011.0685

Guo, J., Haehnle, B., Hoenders, D., Creusen, G., Jiao, D., Kuehne, A. J. C., et al. (2020). Biodegradable laser arrays self-assembled from plant resources. *Adv. Mater.* 32 (29), 2002332. doi:10.1002/adma.202002332

Guo, J. K., Hong, S., Yoon, H., Babakhanova, G., Lavrentovich, O. D., and Song, J. (2019b). Laser-induced nanodroplet injection and reconfigurable double emulsions with designed inner structures. *Adv. Sci.* 6 (17), 1900785. doi:10.1002/advs.201900785

Guo, Q., Yan, K., Chigrinov, V., Zhao, H., and Tribelsky, M. (2019a). Ferroelectric liquid crystals: physics and applications. *Crystals* 9 (9), 470. doi:10.3390/cryst9090470

Haase, W., Podgornov, F., Matsuhisa, Y., and Ozaki, M. (2007). Lasing in dye-doped chiral liquid crystals: influence of defect modes. *Phys. status solidi (a)* 204 (11), 3768–3776. doi:10.1002/pssa.200776415

Hrozhyk, U. A., Serak, S., Tabiryan, N., and Bunning, T. (2007). Optical tuning of the reflection of cholesterics doped with azobenzene liquid crystals. *Adv. Funct. Mater.* 17 (11), 1735–1742. doi:10.1002/adfm.200600776

Hu, J. Y., Xia, C., Fu, D., Zhang, C., Yao, L., Lu, C., et al. (2019). Thermally tunable and electrically switchable solid sphere shell three-layer 3D Bragg microcavity laser based on cholesteric-liquid-crystals. *Appl. Phys. Express* 12 (10), 102017. doi:10.7567/1882-0786/ab45c7

Huang, J.-C., Hsiao, Y. C., Lin, Y. T., Lee, C. R., and Lee, W. (2016). Electrically switchable organo–inorganic hybrid for a white-light laser source. *Sci. Rep.* 6 (1), 28363. doi:10.1038/srep28363

Huang, Y., Zhou, Y., Doyle, C., and Wu, S. T. (2006). Tuning the photonic band gap in cholesteric liquid crystals by temperature-dependent dopant solubility. *Opt. Express* 14 (3), 1236–1242. doi:10.1364/oe.14.001236

Huang, Y. X., Zhang, X., Yu, B., Ma, J., Xie, K., Cheng, S., et al. (2021). Waveguided nematic liquid crystal random lasers. *Nanophotonics* 10 (13), 3541–3547. doi:10.1515/nanoph-2021-0353

Hur, S. T., Lee, B. R., Gim, M., Park, K., Song, M. H., and Choi, S. (2013). Liquid-crystalline blue phase laser with widely tunable wavelength. *Adv. Mater* 25 (21), 3002–3006. doi:10.1002/adma.201204591

Ilchishin, I. P., Tikhonov, E. A., Tishchenko, V. G., and Shpak, M. T. (1980). Generation of a tunable radiation by impurity cholesteric liquid crystals. *Jetp Lett.* 32 (1), 24–27. doi:10.1541/ieejeiss.130.1891

Kasano, M., Ozaki, M., Yoshino, K., Ganzke, D., and Haase, W. (2003). Electrically tunable waveguide laser based on ferroelectric liquid crystal. *Appl. Phys. Lett.* 82 (23), 4026–4028. doi:10.1063/1.1580992

Khan, A. A., Morris, S. M., Gardiner, D. J., Qasim, M. M., Wilkinson, T. D., and Coles, H. J. (2015). Improving the stability of organosiloxane smectic A liquid crystal random lasers using redox dopants. *Opt. Mater.* 42, 441–448. doi:10.1016/j.optmat.2015.02.002

Khoo, I. C. (2014). Nonlinear optics, active plasmonics and metamaterials with liquid crystals. *Prog. Quantum Electron.* 38 (2), 77–117. doi:10.1016/j.pquantelec.2014.03.001

Khoo, I.-C. (2022). *Liquid crystals*. John Wiley and Sons.

Kim, K., Hur, S. T., Kim, S., Jo, S. Y., Lee, B. R., Song, M. H., et al. (2015). A well-aligned simple cubic blue phase for a liquid crystal laser. *J. Mater. Chem. C* 3 (21), 5383–5388. doi:10.1039/c5tc00420a

Kopp, V., Fan, B., Vithana, H. K. M., and Genack, A. Z. (1998). Low-threshold lasing at the edge of a photonic stop band in cholesteric liquid crystals. *Opt. Lett.* 23 (21), 1707–1709. doi:10.1364/ol.23.001707

Korenjak, Z., and Humar, M. (2024). Smectic and soap bubble optofluidic lasers. *Phys. Rev. X* 14 (1), 011002. doi:10.1103/physrevx.14.011002

Lagerwall, J. P., and Scalia, G. (2016). Liquid crystals with nano and microparticles (in 2 volumes). Vol. 7. *World Sci*.

Lagerwall, J. P. F., Schütz, C., Salajkova, M., Noh, J., Hyun Park, J., Scalia, G., et al. (2014). Cellulose nanocrystal-based materials: from liquid crystal self-assembly and glass formation to multifunctional thin films. *NPG Asia Mater.* 6 (1), e80. doi:10.1038/am.2013.69

Lee, C. R., Lin, S. H., Guo, J. W., Lin, J. D., Lin, H. L., Zheng, Y. C., et al. (2015). Electrically and thermally controllable nanoparticle random laser in a well-aligned dye-doped liquid crystal cell. *Opt. Mater. Express* 5 (6), 1469–1481. doi:10.1364/ome.5.001469

Lehmann, O. (1889). Über fliessende krystalle. *Z. für Phys. Chem.* 4 (1), 462–472. doi:10.1515/zpch-1889-0434

Li, L. W. (2017). Random lasers tuning by combining a dye-doped liquid crystal and CdS nanoparticles. *Optik* 134, 1–8. doi:10.1016/j.ijleo.2017.01.031

Liao, R., Zhan, X., Xu, X., Liu, Y., Wang, F., and Luo, D. (2019). Spatially and electrically tunable random lasing based on a polymer-stabilised blue phase liquid crystal-wedged cell. *Liq. Cryst.* 47 (5), 715–722. doi:10.1080/02678292.2019.1673842

Lin, J. D., Wang, T. Y., Mo, T. S., Huang, S. Y., and Lee, C. R. (2016). Wide-band spatially tunable photonic bandgap in visible spectral range and laser based on a polymer stabilized blue phase. *Sci. Rep.* 6, 30407. doi:10.1038/srep30407

Lin, J. H., and Hsiao, Y. L. (2014). Manipulation of the resonance characteristics of random lasers from dye-doped polymer dispersed liquid crystals in capillary tubes. *Opt. Mater. Express* 4 (8), 1555–1563. doi:10.1364/ome.4.001555

Lin, J.-H., Shih, W. C., Xie, Z. H., Tsay, S. Y., and Huang, C. C. (2024). Thermal control band-edge lasing toward near IR from dye-doped cholesteric liquid crystal: relatively stable operation at high temperatures. *Opt. and Laser Technol.* 174, 110592. doi:10.1016/j.optlastec.2024.110592

Lin, S. H., Chen, P. Y., Li, Y. H., Chen, C. H., Lin, J. H., Chen, Y. H., et al. (2017a). Manipulation of polarized random lasers from dye-doped twisted nematic liquid crystals within wedge cells. *Ieee Photonics J.* 9 (2), 1–8. doi:10.1109/jphot.2017.2689064

Lin, T.-H., Chen, Y. J., Wu, C. H., Fuh, A. Y. G., Liu, J. H., and Yang, P. C. (2005). Cholesteric liquid crystal laser with wide tuning capability. *Appl. Phys. Lett.* 86 (16). doi:10.1063/1.1897439

Lin, T.-H., Jau, H. C., Chen, C. H., Chen, Y. J., Wei, T. H., Chen, C. W., et al. (2006). Electrically controllable laser based on cholesteric liquid crystal with negative dielectric anisotropy. *Appl. Phys. Lett.* 88 (6). doi:10.1063/1.2168259

Lin, Y.-L., Gong, L. L., Che, K. J., Li, S. S., Chu, C. X., Cai, Z. P., et al. (2017b). Competitive excitation and osmotic-pressure-mediated control of lasing modes in cholesteric liquid crystal microshells. *Appl. Phys. Lett.* 110 (22). doi:10.1063/1.4984743

Liu, Y. J., Cai, W. F., Li, Y., Tang, Z. Y., He, H. L., Wang, J. W., et al. (2021). Liquid crystal random laser: principles and research progresses. *Chin. J. Lasers-Zhongguo Jiguang* 48 (12). doi:10.3788/cjl202148.1201006

Lu, H., Yang, L., Xia, L., Kong, J., Xu, M., Zhu, J., et al. (2021). Band-edge-enhanced tunable random laser using a polymer-stabilised cholesteric liquid crystal. *Liq. Cryst.* 48 (2), 255–262. doi:10.1080/02678292.2020.1774085

Lu, H. B., Xing, J., Wei, C., Xia, J., Sha, J., Ding, Y., et al. (2018a). Band-gap-tailored random laser. *Photonics Res.* 6 (5), 390–395. doi:10.1364/prj.6.000390

Lu, Y. L., Yang, Y., Wang, Y., Wang, L., Ma, J., Zhang, L., et al. (2018b). Tunable liquid-crystal microshell-laser based on whispering-gallery modes and photonic band-gap mode lasing. *Opt. Express* 26 (3), 3277–3285. doi:10.1364/oe.26.003277

Maiman, T. H. (1960). Stimulated optical radiation in ruby. 187, 493, 494. doi:10.1038/187493a0

Manda, R., Pagidi, S., Heo, Y., Lim, Y. J., Kim, M., and Lee, S. H. (2020). Electrically tunable photonic band gap structure in monodomain blue-phase liquid crystals. *NPG Asia Mater.* 12 (1), 42. doi:10.1038/s41427-020-0225-8

Martinot-lagarde, P., Duke, R., and Durand, G. (2011). Tempearture dependence of tilt, pitch and polarization in ferroelectric liquid crystals. *Mol. Cryst. Liq. Cryst.* 75 (1), 249–286. doi:10.1080/00268948108073619

Matsuhisa, Y., Haase, W., Fujii, A., and Ozaki, M. (2006a). Lowering lasing threshold in ferroelectric liquid crystal sandwiched between dielectric multilayers. *Appl. Phys. Lett.* 89 (20). doi:10.1063/1.2369539

Matsuhisa, Y., Huang, Y., Zhou, Y., Wu, S. T., Ozaki, R., Takao, Y., et al. (2007). Low-threshold and high efficiency lasing upon band-edge excitation in a cholesteric liquid crystal. *Appl. Phys. Lett.* 90 (9). doi:10.1063/1.2710777

Matsuhisa, Y., Ozaki, R., Haase, W., Yoshino, K., and Ozaki, M. (2006b). Light localization and lasing characteristics in one-dimensional photonic crystal with a helix defect of ferroelectric liquid crystal. *Ferroelectrics* 344 (1), 239–245. doi:10.1080/00150190600968371

Matsui, T., Ozaki, R., Funamoto, K., Ozaki, M., and Yoshino, K. (2002). Flexible mirrorless laser based on a free-standing film of photopolymerized cholesteric liquid crystal. *Appl. Phys. Lett.* 81 (20), 3741–3743. doi:10.1063/1.1522498

Mazzulla, A., Petriashvili, G., Matranga, M. A., De Santo, M. P., and Barberi, R. (2012). Thermal and electrical laser tuning in liquid crystal blue phase I. *Soft Matter* 8 (18), 4882. doi:10.1039/c2sm25197c

Meng, Z. Z., Yang, Y., and Wan, Y. (2022). Controllable random lasers based on two-dimensional random gain systems with nematic liquid crystals. *Indian J. Phys.* 96 (6), 1805–1812. doi:10.1007/s12648-021-02109-x

Meyer, R. B., Liebert, L., Strzelecki, L., and Keller, P. (1975). Ferroelectric liquid crystals. *J. de Physique Lettres* 36 (3), 69–71. doi:10.1051/jphyslet:0197500360306900

Milonni, P. W., and Eberly, J. H. (2010). *Laser physics*. John Wiley and Sons.

Mitov, M. (2017). Cholesteric liquid crystals in living matter. *Soft matter* 13 (23), 4176–4209. doi:10.1039/c7sm00384f

Mysliwiec, J., Szukalska, A., Szukalski, A., and Sznitko, L. (2021). Liquid crystal lasers: the last decade and the future. *Nanophotonics* 10 (9), 2309–2346. doi:10.1515/nanoph-2021-0096

Nagai, Y., Shao-Chieh, C., and Kajikawa, K. (2017). Two-dimensional coherent random laser in photonic crystal fiber with dye-doped nematic liquid crystal. *Appl. Opt.* 56 (32), 8969–8972. doi:10.1364/ao.56.008969

Nambiar, K. (2006). *Lasers: principles, types and applications*. Daryaganj, New Delhi: New Age International.

Naruta, T., Akita, T., Uchida, Y., Lisjak, D., Mertelj, A., and Nishiyama, N. (2019). Magnetically controllable random laser in ferromagnetic nematic liquid crystals. *Opt. Express* 27 (17), 24426–24433. doi:10.1364/oe.27.024426

Ozaki, M., Kasano, M., Funamoto, K., Ozaki, R., Matsui, T., and Yoshino, K. (2004). Tunable lasing in doped liquid crystals with one-dimensional periodic structure. *Liq. Cryst. VII*. SPIE5213, 111–122. doi:10.1117/12.509184

Ozaki, M., Kasano, M., Ganzke, D., Haase, W., and Yoshino, K. (2002). Mirrorless lasing in a dye-doped ferroelectric liquid crystal. *Adv. Mater.* 14 (4), 306–309. doi:10.1002/1521-4095(20020219)14:4<306::aid-adma306>3.0.co;2-1

Padiyakkuth, N., Thomas, S., Antoine, R., and Kalarikkal, N. (2022). Recent progress and prospects of random lasers using advanced materials. *Mater. Adv.* 3 (17), 6687–6706. doi:10.1039/d2ma00221c

Palffy-Muhoray, P., and Taheri, B. (2001). Ultraviolet lasing in cholesteric liquid crystals. *Opt. Lett.* 26 (11), 804–806. doi:10.1364/ol.26.000804

Papič, M., Mur, U., Zuhail, K. P., Ravnik, M., Muševič, I., and Humar, M. (2021). Topological liquid crystal superstructures as structured light lasers. *Proc. Natl. Acad. Sci.* 118 (49), e2110839118. doi:10.1073/pnas.2110839118

Perumbilavil, S., Kauranen, M., and Assanto, G. (2018a). Magnetic steering of beam-confined random laser in liquid crystals. *Appl. Phys. Lett.* 113 (12). doi:10.1063/1.5052272

Perumbilavil, S., Kauranen, M., and Assanto, G. (2018c). Near-infrared switching of light-guided random laser. *Ieee Photonics J.* 10 (5), 1–7. doi:10.1109/jphot.2018.2870739

Perumbilavil, S., Kauranen, M., and Assanto, G. (2019). Spatiospectral features of a soliton-assisted random laser in liquid crystals. *Opt. Lett.* 44 (14), 3574–3577. doi:10.1364/ol.44.003574

Perumbilavil, S., Piccardi, A., Barboza, R., Buchnev, O., Kauranen, M., Strangi, G., et al. (2018d). Beaming random lasers with soliton control. *Nat. Commun.* 9, 3863. doi:10.1038/s41467-018-06170-9

Perumbilavil, S., Piccardi, A., Buchnev, O., Kauranen, M., Strangi, G., and Assanto, G. (2017). All-optical guided-wave random laser in nematic liquid crystals. *Opt. Express* 25 (5), 4672–4679. doi:10.1364/oe.25.004672

Perumbilavil, S., Piccardi, A., Buchnev, O., Strangi, G., Kauranen, M., and Assanto, G. (2018b). Spatial solitons to mold random lasers in nematic liquid crystals Invited. *Opt. Mater. Express* 8 (12), 3864–3878. doi:10.1364/ome.8.003864

Popova, M., Bretz, S. L., and Hartley, C. S. (2016). Visualizing molecular chirality in the organic chemistry laboratory using cholesteric liquid crystals. *J. Chem. Educ.* 93 (6), 1096–1099. doi:10.1021/acs.jchemed.5b00704

Qu, D., Archimi, M., Camposeo, A., Pisignano, D., and Zussman, E. (2021). Circularly polarized laser with chiral nematic cellulose nanocrystal cavity. *ACS Nano* 15 (5), 8753–8760. doi:10.1021/acsnano.1c01001

Qu, G., Zhang, X., Li, S., Lu, L., Gao, J., Yu, B., et al. (2023a). Liquid crystal random lasers. *Phys. Chem. Chem. Phys.* 25 (1), 48–63. doi:10.1039/d2cp02859j

Qu, G. Y., Zhang, X., Lu, L., Li, S., Du, W., Cao, Z., et al. (2023b). Efficient and tunable liquid crystal random laser based on plasmonic-enhanced FRET. *Apl. Photonics* 8 (6). doi:10.1063/5.0134978

Reinitzer, F. (1888). Beiträge zur kenntniss des cholesterins. *Monatsh. für Chem. verwandte Teile anderer Wiss.* 9 (9), 421–441. doi:10.1007/bf01516710

Sala-Tefelska, M. M., Orzechowski, K., Sierakowski, M., Siarkowska, A., Woliński, T., Strzeżysz, O., et al. (2018). Influence of cylindrical geometry and alignment layers on the growth process and selective reflection of blue phase domains. *Opt. Mater.* 75, 211–215. doi:10.1016/j.optmat.2017.10.024

Sapienza, R. (2019). Determining random lasing action. *Nat. Rev. Phys.* 1 (11), 690–695. doi:10.1038/s42254-019-0113-8

Scarangella, A., Soldan, V., and Mitov, M. (2020). Biomimetic design of iridescent insect cuticles with tailored, self-organized cholesteric patterns. *Nat. Commun.* 11 (1), 4108. doi:10.1038/s41467-020-17884-0

Schawlow, A. L., and Townes, C. H. (1958). Infrared and optical masers. *Phys. Rev.* 112 (6), 1940–1949. doi:10.1103/physrev.112.1940

Schmidtke, J., Kniesel, S., and Finkelmann, H. (2005). Probing the photonic properties of a cholesteric elastomer under biaxial stress. *Macromolecules* 38 (4), 1357–1363. doi:10.1021/ma0487655

Schmidtke, J., Stille, W., and Finkelmann, H. (2003). Defect mode emission of a dye doped cholesteric polymer network. *Phys. Rev. Lett.* 90 (8), 083902. doi:10.1103/physrevlett.90.083902

Schmidtke, J., Stille, W., Finkelmann, H., and Kim, S. (2002). Laser emission in a dye doped cholesteric polymer network. *Adv. Mater.* 14 (10), 746. doi:10.1002/1521-4095(20020517)14:10<746::aid-adma746>3.0.co;2-5

Seago, A. E., Brady, P., Vigneron, J. P., and Schultz, T. D. (2009). Gold bugs and beyond: a review of iridescence and structural colour mechanisms in beetles (Coleoptera). *J. R. Soc. Interface* 6 (Suppl. l_2), S165–S184. doi:10.1098/rsif.2008.0354.focus

Shang, Z. Z., Wang, Z., and Dai, G. (2023). Stability-enhanced emission based on biophotonic crystals in liquid crystal random lasers. *Materials* 16 (1), 200. doi:10.3390/ma16010200

Sharma, V., Crne, M., Park, J. O., and Srinivasarao, M. (2014). Bouligand structures underlie circularly polarized iridescence of scarab beetles: a closer view. *Mater. Today Proc.* 1, 161–171. doi:10.1016/j.matpr.2014.09.019

Shasti, M., Coutino, P., Mukherjee, S., Varanytsia, A., Smith, T., Luchette, A. P., et al. (2016). Reverse mode switching of the random laser emission in dye doped liquid crystals under homogeneous and inhomogeneous electric fields. *Photonics Res.* 4 (1), 7–12. doi:10.1364/prj.4.000007

Shibaev, P., Kopp, V., and Genack, A. (2003). Photonic materials based on mixtures of cholesteric liquid crystals with polymers. *J. Phys. Chem. B* 107 (29), 6961–6964. doi:10.1021/jp0222189

Shirvani-Mahdavi, H., and Ebrahimi-Azandariani, S. (2019). Effect of combined laser dyes on the efficiency of cholesteric liquid crystal lasers. *J. Theor. Appl. Phys.* 13 (1), 7–15. doi:10.1007/s40094-019-0318-3

Siegman, A. E. (1986). *Lasers*. Sausalito, CA, United States: University science books.

Svelto, O., and Hanna, D. C. (2010). *Principles of lasers. Vol. 1*. Springer.

Sznitko, L., Kaliciak, K., Adamow, A., and Mysliwiec, J. (2016). A random laser made of nematic liquid crystal doped with a laser dye. *Opt. Mater.* 56, 121–128. doi:10.1016/j.optmat.2015.10.029

Szukalska, A., and Mysliwiec, J. (2023). White lasing–materials, design and applications. *J. Mater. Chem. C* 11 (26), 8724–8757. doi:10.1039/d3tc00872j

Tao, J., Li, J., Yu, X., Wei, L., and Xu, Y. (2021). Lateral gradient ambidextrous optical reflection in self-organized left-handed chiral nematic cellulose nanocrystals films. *Front. Bioeng. Biotechnol.* 9, 608965. doi:10.3389/fbioe.2021.608965

Tiwari, A. K., Pattelli, L., Torre, R., and Wiersma, D. S. (2018). Remote control of liquid crystal elastomer random laser using external stimuli. *Appl. Phys. Lett.* 113 (1). doi:10.1063/1.5038663

Trull, J., Salud, J., Diez-Berart, S., and López, D. O. (2017). Influence of liquid crystalline phases on the tunability of a random laser. *Phys. Rev. E* 95 (5), 052704. doi:10.1103/physreve.95.052704

Turitsyn, S. K., Babin, S. A., Churkin, D. V., Vatnik, I. D., Nikulin, M., and Podivilov, E. V. (2014). Random distributed feedback fibre lasers. *Phys. Reports-Review Sect. Phys. Lett.* 542 (2), 133–193. doi:10.1016/j.physrep.2014.02.011

Uchimura, M., Watanabe, Y., Araoka, F., Watanabe, J., Takezoe, H., and Konishi, G. (2010). Development of laser dyes to realize low threshold in dye-doped cholesteric liquid crystal lasers. *Adv. Mater* 22 (40), 4473–4478. doi:10.1002/adma.201001046

Unser, S., Bruzas, I., He, J., and Sagle, L. (2015). Localized surface plasmon resonance biosensing: current challenges and approaches. *Sensors* 15 (7), 15684–15716. doi:10.3390/s150715684

Varanytsia, A., Guo, T., and Palffy-Muhoray, P. (2019). Small footprint cholesteric liquid crystal laser. *Appl. Opt.* 58 (4), 739–743. doi:10.1364/ao.58.000739

Varanytsia, A., Nagai, H., Urayama, K., and Palffy-Muhoray, P. (2015). Tunable lasing in cholesteric liquid crystal elastomers with accurate measurements of strain. *Sci. Rep.* 5, 17739. doi:10.1038/srep17739

Wan, Y., and Deng, L. G. (2020). Pump-controlled plasmonic random lasers from dye-doped nematic liquid crystals with TiN nanoparticles in non-oriented cells. *Appl. Sciences-Basel* 10 (1), 199. doi:10.3390/app10010199

Wan, Y., Wang, H., Li, H., Ye, R., Zhang, X., Lyu, J., et al. (2022). Low-threshold random lasers enhanced by titanium nitride nanoparticles suspended randomly in gain solutions. *Opt. Express* 30 (5), 8222–8233. doi:10.1364/oe.451428

Wang, C. L., Gong, C., Zhang, Y., Qiao, Z., Yuan, Z., Gong, Y., et al. (2021). Programmable rainbow-colored optofluidic fiber laser encoded with topologically structured chiral droplets. *Acs Nano* 15 (7), 11126–11136. doi:10.1021/acsnano.1c02650

Wang, J. L., Zhang, Y., Cao, M., Song, X., Che, Y., Zhang, H., et al. (2016). Platinum-scatterer-based random lasers from dye-doped polymer-dispersed liquid crystals in capillary tubes. *Appl. Opt.* 55 (21), 5702–5706. doi:10.1364/ao.55.005702

Wang, M., Zou, C., Sun, J., Zhang, L., Wang, L., Xiao, J., et al. (2017). Fluorescent nanomaterials for the development of latent fingerprints in forensic sciences. *Adv. Funct. Mater.* 27 (46), 1606243. doi:10.1002/adfm.201606243

Wang, Z., Cao, M., Shao, G., Zhang, Z., Yu, H., Chen, Y., et al. (2020a). Coherent random lasing in colloidal quantum dot-doped polymer-dispersed liquid crystal with low threshold and high stability. *J. Phys. Chem. Lett.* 11 (3), 767–774. doi:10.1021/acs.jpclett.9b03409

Wang, Z. Y. H., Zhang, Y., Gong, X., Yuan, Z., Feng, S., Xu, T., et al. (2020b). Bio-electrostatic sensitive droplet lasers for molecular detection. *Nanoscale Adv.* 2 (7), 2713–2719. doi:10.1039/d0na00107d

Wei, G., Feng, K., Ma, S., Jiang, Y., and Jin, Z. (2023). Exploring the core parameters of CNC-based chiral nematic structures for enhancing the dissymmetry factor of right-handed circularly polarized luminescence. *ACS omega* 8 (25), 23191–23201. doi:10.1021/acsomega.3c02969

Wilts, B. D., Whitney, H. M., Glover, B. J., Steiner, U., and Vignolini, S. (2014). Natural helicoidal structures: morphology, self-assembly and optical properties. *Mater. Today Proc.* 1, 177–185. doi:10.1016/j.matpr.2014.09.021

Woska, S., Münchinger, A., Beutel, D., Blasco, E., Hessenauer, J., Karayel, O., et al. (2020). Tunable photonic devices by 3D laser printing of liquid crystal elastomers. *Opt. Mater. Express* 10 (11), 2928–2935. doi:10.1364/ome.402855

Xie, R. C., Tsay, S. Y., Wu, J. J., Kuo, C. C., Zhang, H., and Lin, J. H. (2022). Manipulation of plasmonic random laser from dye-doped liquid crystals inside photonic crystal fiber by the electric field. *Opt. Laser Technol.* 151, 108013. doi:10.1016/j.optlastec.2022.108013

Yang, T. H., Chen, C. W., Jau, H. C., Feng, T. M., Wu, C. W., Wang, C. T., et al. (2019). Liquid-crystal random fiber laser for speckle-free imaging. *Appl. Phys. Lett.* 114 (19). doi:10.1063/1.5094887

Yao, F. F., Bian, H., Pei, Y., Hou, C., and Sun, X. (2016). Behaviors of random laser in dye-doped nematic liquid crystals. *Opt. Commun.* 359, 15–19. doi:10.1016/j.optcom.2015.09.053

Yao, F., Zhang, C., Zhou, Y., Song, Z., Pei, Y., Wang, J., et al. (2023). Control over polarization of vertically emitting random lasers based on dye doped nematic liquid crystals by applying a transverse electric field locally. *Opt. Laser Technol.*, 161. doi:10.1016/j.optlastec.2023.109215

Ye, L. H., Liu, B., Li, F., Feng, Y., Cui, Y., and Lu, Y. (2016). The influence of Ag nanoparticles on random laser from dye-doped nematic liquid crystals. *Laser Phys. Lett.* 13 (10), 105001. doi:10.1088/1612-2011/13/10/105001

Ye, L. H., Liu, B., Zhao, C., Wang, Y., Cui, Y., and Lu, Y. (2014). The electrically and magnetically controllable random laser from dye-doped liquid crystals. *J. Appl. Phys.* 116 (5). doi:10.1063/1.4891683

Ye, L. H., Lv, C., Wang, Y., Liu, B., and Cui, Y. (2017b). Effect of alignment layer on polymer-dispersed liquid crystal random laser. *J. Mod. Opt.* 64 (14), 1429–1434. doi:10.1080/09500340.2017.1291864

Ye, L. H., Wang, Y., Feng, Y., Liu, B., Gu, B., Cui, Y., et al. (2018). Thermally switchable photonic band-edge to random laser emission in dye-doped cholesteric liquid crystals. *Laser Phys. Lett.* 15 (3), 035002. doi:10.1088/1612-202x/aa8e85

Ye, L. H., Zhao, C., Feng, Y., Gu, B., Cui, Y., and Lu, Y. (2017a). Study on the polarization of random lasers from dye-doped nematic liquid crystals. *Nanoscale Res. Lett.* 12, 27. doi:10.1186/s11671-016-1778-x

Yokoyama, S., Mashiko, S., Kikuchi, H., Uchida, K., and Nagamura, T. (2005). Laser emission from a polymer-stabilized liquid-crystalline blue phase. *Adv. Mater.* 18 (1), 48–51. doi:10.1002/adma.200501355

Zhang, J. C., Zhu, H. Y., Zhang, Y. L., Zhu, X. M., Wang, Z., Chen, F. L., et al. (2022). Scattering-assisted and logic-controllable WGM laser in liquid crystal micropillar. *J. Light. Technol.* 40 (15), 5216–5223. doi:10.1109/jlt.2022.3176401

Zhang, Y., Gong, X., Yuan, Z., Wang, W., and Chen, Y. C. (2020b). DNA self-switchable microlaser. *ACS Nano* 14 (11), 16122–16130. doi:10.1021/acsnano.0c08219

Zhang, Y. S., Jiang, S., Lin, J., Yang, P., and Lee, C. (2020a). Stretchable freestanding films of 3D nanocrystalline blue phase elastomer and their tunable applications. *Adv. Opt. Mater.* 9 (1). doi:10.1002/adom.202001427

Zhao, L. Y., Wang, Y., Yuan, Y., Liu, Y., Liu, S., Sun, W., et al. (2017). Whispering gallery mode laser based on cholesteric liquid crystal microdroplets as temperature sensor. *Opt. Commun.* 402, 181–185. doi:10.1016/j.optcom.2017.06.008

Zhao, S., Zhu, H., Lu, J., Li, M., Zhao, L., Zhou, L., et al. (2022). Uncovering the origin of chirality from plasmonic nanoparticle/cellulose nanocrystal composite films. *Adv. Funct. Mater.* 32 (44), 2201927. doi:10.1002/adfm.202201927

Zhou, D., Zhao, N., Chen, Y., Sun, J., Li, Y., Peng, Z., et al. (2023). Laser emission from tapered fiber-based liquid-crystal microsphere for sensing. *Opt. Lett.* 48 (14), 3773–3776. doi:10.1364/ol.492930

Zhou, L., Fu, H., Lv, T., Wang, C., Gao, H., Li, D., et al. (2020). Nonlinear optical characterization of 2D materials. *Nanomaterials* 10 (11), 2263. doi:10.3390/nano10112263

Zhu, J. L., Li, W. H., Sun, Y., Lu, J. G., Song, X. L., Chen, C. Y., et al. (2015). Random laser emission in a sphere-phase liquid crystal. *Appl. Phys. Lett.* 106 (19). doi:10.1063/1.4921325

Zhu, X., He, Z., Zhu, H., and Zhang, W. (2023). Spectrally programmable fiber microcavity laser with dye-doped liquid crystals. *Opt. Laser Technol.* 158, 108860. doi:10.1016/j.optlastec.2022.108860